Comparison of Simulated and Observed Severe Storm Tracks over Alberta

by

Lindsay Ruth Sutton

A thesis submitted in partial fulfilment of the requirements for the degree of

Master of Science

Department of Earth and Atmospheric Sciences
University of Alberta

Abstract

Thunderstorms have the potential to produce severe weather and can result in significant financial and human losses. The province of Alberta is one of Canada's most active thunderstorm regions, with the record for insured damage due to hail. Therefore, it is crucial that thunderstorm forecasts be as accurate as possible to provide early warning to industry and the public.

Numerical Weather Prediction (NWP) models are heavily utilized to provide forecast guidance. Recent advances in computing power and affordability have enabled the use of finer spatial resolutions that allow for the explicit simulation of individual storms, that is, without the use of a cumulus parameterization scheme. There is a need to explore the forecast skill of these high-resolution models as they find their way into forecast operations.

This thesis investigates the skill of the widely available Weather Research and Forecasting (WRF) model for predicting the motion of thunderstorms. We use a 4 km resolution, a value that is found to be sufficient for accurately reproducing storm structure and evolution without requiring too many computational resources. Our focus is on a select set of severe summer storms that occurred in Alberta during 2011 and 2012. We compare the WRF simulated and observed radar reflectivity values and present the differences, with an emphasis on the motion and intensity of the storms. We find that storms produced by the WRF model move faster, travel farther, and have more counter clockwise tracks than radar-observed storms. WRF storms are also found to be less intense in terms of reflectivity (dBZ).

We also investigate the accuracy of the Traditional Method and Bunkers Method for forecasting storm motion. These methods are frequently used by forecasters because they are relatively easy to employ on an observed or model sounding, and there is no need to rely on the results of a high-resolution model. We find that both methods tend to underestimate storm speed and overestimate storm direction when used on WRF model forecast soundings over Alberta.

Acknowledgements

This thesis could not have been completed without the raw radar data and metadata provided by Dave Patrick from the Prairie and Arctic Storm Prediction Centre (PASPC) of Environment Canada. His knowledge of Environment Canada's radars was crucial to my understanding and manipulation of the data. Also, thank you to the Meteorological Service of Canada for access to historical radar imagery and Severe Weather Event Database (SWED) reports.

My sincerest thanks goes to my supervisor Gerhard Reuter for his guidance. Fellow graduate students Daniel Brown and Clark Pennelly were also very generous in their willingness to guide me through the use of WRF-EMS and to provide insight on the many technical and research related questions that I had. Also, thanks to Bruno Larochelle for proofreading my thesis, and to Kerri-Ann Munchinsky and Michelle Johnson for the continued motivation offered over many lunch dates!

I gratefully acknowledge financial support from the National Science and Engineering Research Council of Canada, Environment Canada, and the province of Alberta.

Table of Contents

List of Tables

List of Figures

Abbreviations

ARW	Advanced Research WRF
CAPE	Convective available potential energy
CAPPI	Constant Altitude Plan Position Indicator
CARDS	Canadian Radar Decision Support system
dBZ	Decibels relative to Z
EMS	Environmental Modeling System
GRIB	Gridded Binary
IDW	Inverse Distance Weighting
MDT	Mountain Daylight Time
NARR	North American Regional Reanalysis
NCAR	National Center for Atmospheric Research
NMM	Nonhydrostatic Mesoscale Model
NOAA	National Oceanic and Atmospheric Administration
NWP	Numerical Weather Prediction
NWS	National Weather Service
PASPC	Prairie and Arctic Storm Prediction Centre
SCIT	Storm Cell Identification and Tracking
SWED	Severe Weather Event Database
TITAN	Thunderstorm Identification, Tracking, Analysis, and Nowcasting
URP	Unified Radar Processing
UTC	Coordinated Universal Time
WRF	Weather Research and Forecasting
WRF-EMS	Weather Research and Forecasting Model - Environmental Modeling System
WSE	Upper air sounding site at Stony Plain, Alberta
Z	Effective radar reflectivity
30R75	Traditional Method

Chapter 1

Introduction

1.1 Severe thunderstorms over Alberta

Thunderstorms have the potential to produce hazardous weather conditions such as hail, lightning, torrential rainfall, strong wind, and tornadoes. These hazards can result in significant financial and human losses. The regions of central and southern Alberta, Canada are particularly prone to summer severe weather. About 13 tornadoes per year per 10000 km^2 occur in south-central Alberta (Paruk and Blackwell 1994). The Alberta foothills region experiences the greatest number of lightning events in Canada with 45 days per year, as well as the longest duration of lightning with 18.25 hours per year (Burrows et al. 2002). Southern Alberta also records an average of 51 hail days each summer, 11 of which are considered severe with hail larger than golf balls (Smith et al. 1998). A thunderstorm that passed over Calgary, Alberta on 12 July 2010 dropped copious amounts of golf ball sized hail (45 mm diameter) and caused over $400 million in insured damages. This set a new Canadian record for insured damage due to hail, surpassing the previous record of $342 million caused by a hailstorm in Calgary in 1991 (McMurray 2010).

In June 2013 Calgary made media headlines once again as large sections of the city were flooded when the Bow and Elbow rivers overflowed their banks after heavy rain. About 75000 people were displaced (Ogrodnik 2013). This event, combined with devastating flooding along most rivers in southern Alberta, caused over $1.7 billion in insured property damage and the deaths of five people (The Canadian Press 2013, Calgary Herald 2014). Because of the potentially devastating impacts of thunderstorms and summer severe weather, it is important that forecasts be as accurate as possible to provide early warning to businesses, emergency services, and the public.

Numerical Weather Prediction (NWP) models are heavily utilized in operational forecasting to provide forecast guidance. Since their introduction in the mid-20^{th}

century, NWP models have gained about one day of forecast skill each decade and have produced an increasingly accurate representation of the atmosphere (EC 2014). Recent advances in computing power and affordability have enabled the use of finer model grid resolutions that allow for the simulation of individual convective storms. It is expected that these models will contribute to the continued increase in forecast accuracy and result in greatly improved warning lead times for severe weather (Kain et al. 2006, Stensrud et al. 2009). This could prove to be invaluable for protecting lives and property, particularly in storm prone areas such as Alberta.

Research effort on high-resolution models has traditionally focussed on improving the timing of thunderstorm initiation, growth, and dissipation, and the development of hail, rain, and tornadoes from these cells, and little research has focused on examining predicted thunderstorm movement (Fowle and Roebber 2003, Kain et al. 2008, Pennelly 2013). This thesis will focus on investigating this important aspect of thunderstorm forecasting. I will evaluate the accuracy of predicted thunderstorm tracks over Alberta produced by the Weather Research and Forecasting (WRF) model.

1.2 Thunderstorm tracks

1.2.1 Thunderstorm motion on radar

Radar is a primary tool used by weather forecasters for the monitoring, tracking, and nowcasting of thunderstorms. Nowcasting is the term used for the process of describing the current weather and using extrapolation to obtain a short-term forecast for up to 6 hours into the future (PWS 2012). Radar is ideal for nowcasting because it can give frequent and detailed information about the size, shape, and intensity of precipitation regions, as well as their speed and direction of movement. These characteristics are critical for the accurate tracking of severe thunderstorms. To obtain this information, a radar antenna sends out pulses of energy which scatter upon

collision with objects in the atmosphere such as rain and hail. The radar then "listens" for any backscattered energy. The computed time it takes for each reflected energy signal to return to the radar determines how far the precipitation is from the radar, and the intensity of the echoes is analyzed to determine a precipitation rate. The radar reflectivity (Z) is the fraction of power that is returned to the radar and is dependent on the size distribution of the objects (Cain and Kirkwood 2005). It is expressed in dBZ (decibels relative to Z), where the higher the dBZ value the more intense the precipitation is determined to be.

The Marshall-Palmer relationship between radar reflectivity and rainfall rate is

$$Z = 200R^{1.6} \quad (1)$$

where Z is the effective radar reflectivity (mm^6/m^3) and R is the rainfall rate (mm/h) (Marshall et al. 1947). This relationship is used for Canadian radars during the summer, though it performs best for stratiform rain and tends to underestimate convective rainfall rate (Xin et al. 1997).

Images are generated using the calculated dBZ values, and the extrapolation of these radar echoes is one of the key techniques of nowcasting (PWS 2012). Many methods and algorithms have been developed to extrapolate the motion of radar echoes and generate a short-term forecast for their evolution (Wilson and Kessler III 1963, Einfalt et al. 1990, Cheng et al. 1996, Johnson et al. 1998). One such algorithm by Dixon and Wiener (1993) was further developed to produce the TITAN (Thunderstorm Identification, Tracking, Analysis, and Nowcasting) software by researchers at the National Center for Atmospheric Research (NCAR) (RAL 2012). This algorithm uses a variation of the "centroid tracking" method which identifies the center of each storm cell in three dimensions and determines the predicted motion of each radar echo by observing the motion of each storm center on successive radar scans (Dixon and Wiener 1993). The cell tracking and nowcasting algorithms within the Canadian Radar Decision Support system (CARDS) at Environment Canada are based closely on the TITAN method (Patrick and McCarthy 2008). This system is used by forecast offices within the Meteorological Service of Canada and, in combination with Environment Canada's

Unified Radar Processing (URP) software, has proven valuable for forecasting severe summer storms and developing additional nowcasting techniques for thunderstorm-prone areas such as the Prairies and southern Ontario (Yang and King 2010).

1.2.2 Weather models and convection

Though radar tracking methods are extremely valuable for producing short-term forecasts and warnings, they are not employable until a storm is actually detected on radar. In an area showing the potential for storm formation, storm motion must be forecast before a storm develops in order to provide timely warning to residents. Many studies have attempted to define a relationship between storm motion and observed environmental wind speed and direction (Davies and Johns 1993, Sioutas and Flocas 1996, Rasmussen and Blanchard 1998, Bunkers et al. 2000). One commonly used method estimates storm motion to be 30° to the right and 75% of the magnitude of the mean wind in the lowest 6 km of the atmosphere (Maddox 1976). Though this method is relatively simple to employ on wind data obtained from atmospheric soundings and model output, it is an empirical relationship derived from severe storm motion in the eastern United States and it does not accurately forecast storm motion over Alberta (Krauss and Sinkevich 2007B). It also fails to predict the motion of left-moving storms and the acceleration of long-lived storms (Krauss and Sinkevich 2007B).

There are several factors, both internal and external to a storm, that influence storm motion besides the 0-6 km mean wind. These include the interaction between a storm's updraft and the environmental wind shear (Weisman and Klemp 1986), any vertical transfer of momentum within a storm (Krauss and Sinkevich 2007A), the influence of the cold pool on cell propagation (Corfidi 2003), and the merging of neighboring cells (Krauss and Sinkevich 2007A). Given this fact, there needs to be a more flexible and comprehensive method for determining storm motion than those based solely on environmental winds. This is where Numerical Weather Prediction might be of use. Models can take into account many different aspects of the atmosphere,

ground surface, and interaction between thunderstorm cells, and can account for changes in these values with time.

NWP models have improved significantly since their operational forecasting debut in 1955. The first operational model was inaccurate and unreliable, and provided almost no useful information to forecasters; however, it was the beginning of modern NWP, and after extensive refinement and computer development in the next five years the quality of NWP products improved dramatically and rivalled those being produced manually at the National Meteorological Center in the United States (Shuman 1989). Since then, the development of more sophisticated NWP models and more accurate products has been made possible by advances in computer technology, as well as an increasing knowledge of atmospheric physics and the increased frequency and quality of atmospheric observations (Shuman 1989). NWP is now a crucial tool for forecast operations, and forecasters rely heavily on model guidance for accurate forecast production.

Weather forecasters have used numerical model output for many years to help determine the probable location and motion of storms based on predicted environmental variables such as wind speed, wind direction, and humidity (NSSL 2006), but advances in computer power and affordability have led to an increase in the use of high-resolution models as direct forecast tools (Elmore et al. 2002). These “cloud-scale” models use horizontal resolutions that are high enough to explicitly simulate the formation and evolution of convective cells, that is, without the use of a cumulus parameterization scheme. It has been found that a grid spacing of 4 km or finer is sufficient for accurately reproducing the structure, distribution, and evolution of observed storms, with the understanding that the finer the grid spacing the more realistic and detailed the convective structure will be (Done et al. 2004, Erfani et al. 2003, Weisman et al. 1997). There is also evidence that a grid spacing of 2 km adds little more to the overall convective pattern or forecast skill than a 4 km grid, while requiring many more computational resources (Kain et al. 2008, Schwartz et al. 2009). The simulations for this thesis use a 4 km resolution. This value was found to provide a good

compromise between forecast data accuracy and computing time with the resources available.

1.2.3 Lack of research on model thunderstorm tracks

While the prediction of thunderstorm motion remains a crucial component of thunderstorm forecasting, previously conducted research on the convective forecast skill of cloud-scale models has not focussed on thunderstorm tracks. These studies have focussed on aspects such as evaluating a model's skill in forecasting convective initiation (timing and location), the spatial occurrence of precipitation within the forecast domain, and the type of system a storm evolves into (Fowle and Roebber 2003, Kain et al. 2008, Pennelly 2013). It may be argued that NWP models do not have the forecast skill required for a direct assessment of storm tracks, but this is incorrect. Studies by Erfani et al. (2003) and Milbrandt and Yau (2006) on the Pine Lake storm in southwestern Alberta on 14 July 2000 show the skill of explicit high-resolution models in reproducing a storm's motion and speed.

When it comes to comparing the motion of simulated and observed storms, studies often employ a mix of subjective assessment and grid point comparison (Fowle and Roebber 2003, Kain et al. 2008, Schwartz et al. 2009). The latter involves a comparison between forecast accumulated precipitation and observed radar data for each grid point within the forecast domain. Neither of these methods can directly assess and quantify the accuracy of individual storm tracks. There are ways of examining forecast storm motion that would more easily facilitate an examination of storm tracks. A study by Done et al. (2004) on explicit convective forecasts over the central United States attempted to quantify the position errors of storms to determine any directional bias of the WRF model. Position errors in kilometers were calculated for both the east-west and north-south components of model storm tracks that corresponded with observed storms on radar. Errors in storm speed were also noted and analyzed along with position errors to explain the overall propagation error within forecasts.

This thesis will further explore the propagation errors in WRF convective forecasts, focussing specifically on storms over Alberta. This will add to the growing pool of knowledge regarding the convective forecast skill of NWP models which is becoming increasingly important as convection-resolving models find their way into forecast operations.

1.3 Research objectives

The main scientific questions to be answered in this thesis are as follows:

1) How accurately does the WRF model simulate the motion of severe thunderstorms over Alberta?
2) How well do the Traditional Method and Bunkers Method of forecasting storm motion perform when used on WRF model forecast soundings?

1.4 Thesis outline

The first chapter of this thesis provides an introduction to severe thunderstorms over Alberta and the use of radar and model data to forecast storm motion. It also outlines the lack of previous research on model thunderstorm tracks produced by high-resolution models. This is a growing concern given that the availability of high-resolution model data continues to increase, and there remains a need for accurate prediction of thunderstorm motion for the production of timely and effective forecasts. This thesis will help to fill this knowledge gap by investigating the accuracy of thunderstorm tracks over Alberta produced by the WRF model with a resolution of 4 km.

Chapter 2 of this thesis outlines the radar and model data used for this study and explains the steps taken to select appropriate storm days and to produce thunderstorm tracks. Chapter 3 is a case study of the damaging hailstorm in Calgary on 12 August 2012. This case study is presented primarily as an illustration of how the thunderstorm tracks are created and compared in this thesis and how conclusions are obtained. It also

serves to emphasize the potential severity of storms on the Prairies and the importance of timely and accurate thunderstorm forecasts.

A full analysis of the simulated and observed storm tracks is presented in chapter 4 with an emphasis on comparing the motion and intensity of the storms. An investigation into the accuracy of the Traditional Method and Bunkers Method for forecasting storm motion is given in chapter 5, as well as a comparison between the two methods using the data in this study. Chapter 6 gives a summary of this thesis, the conclusions made, as well as suggestions for further research.

Chapter 2

Thunderstorm Track Selection and Generation

2.1 Radar data

The first step towards answering the scientific questions of this study was to determine a set of severe storm days that would allow for a comparison of WRF model output with radar data. A storm "day" for this study consists of the convective activity after 1200 UTC (6:00 am MDT) through until its dissipation before 1200 UTC (6:00 am MDT) the following day. This allows for the capture of one cycle of convective activity each storm "day," typically from initiation in the afternoon of the storm day to dissipation that evening or the following morning. Defining a day like this was done to ease the analysis of each set of thunderstorm tracks and to simplify the execution of the WRF model and the generation of model data for each storm case.

A list of storm days was compiled after examination of historical radar imagery (PRECIP-Rain product) (EC 2013) from Environment Canada for each day from 1 June to 31 August 2011 and 1 June to 31 August 2012. Days were eliminated if they had no storms that initiated in Alberta, no tracks that remained within Canadian radar coverage, or had all storm cells merging into a squall line or other mesoscale feature such as a mesoscale convective system. The latter requirement was implemented in order to prevent the modification of this study's track data by mesoscale convective features. The intent is to focus on the unique motion of individual thunderstorms, not the motion of mesoscale features such as squall lines.

Digital data of CAPPI (Constant Altitude Plan Position Indicator) 1.5 km radar observations was obtained from Environment Canada for each storm day. The CAPPI 1.5 km product was chosen because it gives a horizontal cross section of data at a constant altitude, which is most directly comparable to model output at a specific pressure level. For Alberta's radar sites, the average pressure at 1.5 km above the surface is approximately 750 mb. Maintaining a constant data level aloft also allows for a more

consistent identification of a cell's center as opposed to identifying its location based on precipitation distribution near the surface as given by vertical composite radar products. This can result in a more easily identifiable and consistent track (Koch et al. 2005). Choosing a higher altitude also avoids comparing radar and model data within the atmospheric surface layer, a zone in which there is increased prevalence of radar ground clutter contamination (Koch et al. 2005).

There are five radars in Alberta: Spirit River (near Grande Prairie), Jimmy Lake (near Cold Lake), Carvel (near Edmonton), Strathmore (near Calgary), and Schuler (near Medicine Hat). Figure 2-1 shows the location of these radars in Canada, with the borders of the Prairie Provinces outlined in black. Each radar has a 256 kilometer range. One dBZ value is recorded for each "bin," where a bin has a 1 km radial length and a 1° beam width, so there are 92160 dBZ values for each radar scan. The appropriate radar data for each storm day was retrieved based on the location of the day's storms. In the event that the storm tracks on a specific day extended past the Alberta-Saskatchewan border, data was also retrieved from the two radars in Saskatchewan: Radisson (near Saskatoon) and Bethune (near Regina).

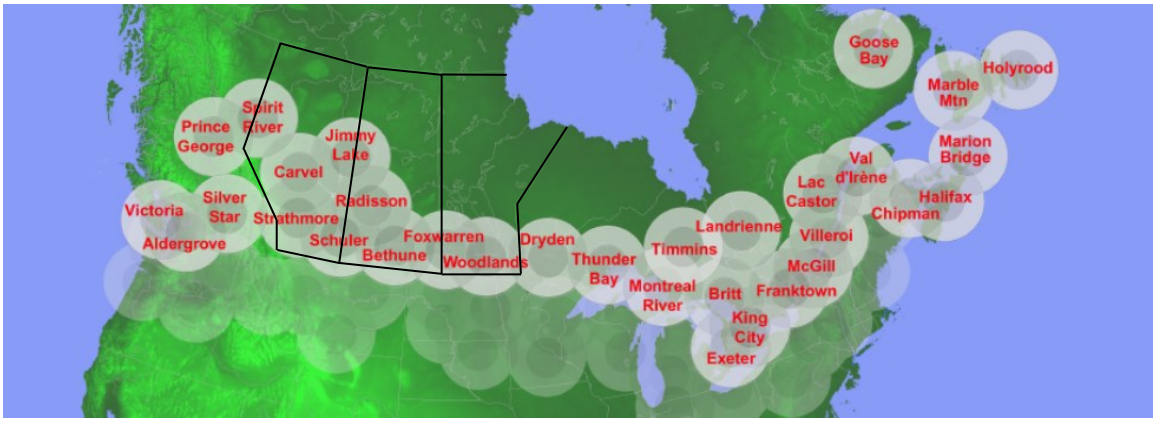

Figure 2-1: A map of the Canadian weather radar network. The borders of the Prairie Provinces are outlined in black. The shading around each radar site indicates 120 km and 240 km range rings, the approximate extent of Doppler and conventional radar products, respectively. Translucent shading to the south indicates the locations of American NEXRAD radars and their spatial coverage (Joe and Lapczak 2002).

Data from each radar was merged into one file per time step for analysis using ArcMap (Esri ArcGIS 10.0). In areas with overlapping radar coverage, the data from the bins closest to a radar center was kept while the rest was discarded. This was done to minimize the negative effects of radar range on the reflectivity values due to beam attenuation, beam spreading, and increasing beam height (Fabry et al. 1992).

A specific set of storm day selection criteria was defined along with a set of thunderstorm track selection criteria. Both lists were required to finalize the set of storm days for this study since the latter list is a required component of the first. Only those days that fulfilled the storm day selection criteria were retained for this study. The following lists give the storm day selection criteria and the storm track selection criteria for the radar data.

Storm day selection criteria

Storm days must

- occur within the summer months (June to August) of 2011 and 2012,
- have more than one thunderstorm track that meets the radar storm track selection criteria,
- have storm cells that do not merge into a squall line or other mesoscale convective feature, and
- have no significant temporal gaps in radar coverage over the storm track location(s) (ie. more than 1 scan missing in a row (more than 10 minutes)).

Radar storm track selection criteria

Each radar storm track must

- be produced by a storm cell with a 35 dBZ area greater than 10 km^2 and having its center at the dBZ weighted mean center,
- start within Alberta and remain within Canadian radar coverage,
- last for at least 6 consecutive radar scans (50 minutes),

- not be missing a 35 dBZ weighted mean center for more than 1 consecutive radar scan (more than 10 minutes) along the length of the track (this could occur if there is missing radar data or the 35 dBZ area is too small or non-existent),
- end before the last radar scan gathered for the storm day, and
- end at the time step before the first scan where the 35 dBZ area is greater than 576 km^2. If this area threshold is reached before the track has met the minimum duration threshold, the track is discarded.

The following procedures are used for storm splits and merges.

- If a storm cell splits into two cells, two tracks are created that share the initial merged part of the track; however, for a track to be included, the second part of the track must last at least 5 consecutive radar scans (40 minutes) and not be missing more than 1 consecutive radar scan (more than 10 minutes) along its length.
- If two storms merge into one cell, the two tracks continue and share the merged part of the track; however, for the tracks to be included, the second part of the track must last at least 5 consecutive radar scans (40 minutes) and not be missing more than 1 consecutive radar scan (more than 10 minutes) along its length.

Key components of the storm track selection criteria include the requirement for a storm to be a discrete cell that initiates within Alberta, achieves and maintains 35 dBZ for at least 50 minutes (6 consecutive radar scans), and remains within Canadian radar coverage for the entirety of its track. The intensity and duration thresholds of 35 dBZ and 50 minutes were chosen to eliminate non-severe thunderstorms as well as severe "pulse" storms that form and dissipate quickly without producing a well-defined track. The value of 35 dBZ is one of the user-defined intensity thresholds suggested for use within the TITAN storm identification algorithm (Han et al. 2009). The requirement that the 35 dBZ area must exceed 10 km^2 was taken from the default value within the SCIT (Storm Cell Identification and Tracking) algorithm that is used to define a storm

component within a storm cell (Johnson 1998). Supercell storms can easily grow to over 25 km in diameter on radar under favorable conditions (Kuster et al. 2012). Therefore, the maximum cell size threshold of 576 km^2 was chosen to allow for the inclusion of these large thunderstorm cells, with an equivalent model size of up to 36 grid spaces at 4 km resolution, while also eliminating storms which are no longer discrete cells.

After the storm day and thunderstorm track selection process was complete, there remained 14 storm days included in this study. Table 2-1 lists these storm days, as well as notable locations of thunderstorm tracks and reported severe weather. The severe weather reports were taken from the Severe Weather Event Database (SWED), which contains weather reports from the public made to the Prairie and Arctic Storm Prediction Centre (PASPC) of Environment Canada. See Table A-1 in Appendix A for conversions between reported hail sizes as referenced to objects and hailstone diameter in millimeters, where applicable.

Table 2-1. The 14 storm days in this study, as well as notable locations of thunderstorm tracks and reported severe weather. See Table A-1 in Appendix A for conversions between reported hail sizes as referenced to objects and hailstone diameter in millimetres.

Storm Day	Notable Storm Location(s)	Reported Severe Weather
11 July 2011	Rocky Mountain House, Lacombe, Dalemead	Heavy rain, marble sized hail, funnel cloud
25 July 2011	Nordegg, Rocky Mountain House, Mayerthorpe	N/A
27 July 2011	Claresholm, Priddis, Granum	Loonie sized hail, funnel cloud
31 July 2011	Ponoka, Buck Lake	Toonie to walnut sized hail
3 August 2011	Calgary, Langdon	Quarter to loonie sized hail, funnel cloud, heavy rain
9 August 2011	Cochrane, Alder Flats	Heavy rain, 1.1 cm hail
14 August 2011	Hamlin, Ranfurley	Loonie to golf ball sized hail
15 August 2011	Sundre, Bassano	80 km/hr winds with gusts to 100 km/hr, pea sized hail
5 July 2012	Calgary, Olds, Millet	Quarter to loonie sized hail, funnel cloud
7 July 2012	Helina, Mallaig	Quarter sized hail, heavy rain
27 July 2012	Nanton, Irricana, Champion, Hill Spring	Ping pong to tennis ball sized hail
4 August 2012	Whitecourt, Calmar, Spruce Grove, Fort Saskatchewan, Sangudo	Strong winds > 100 km/hr, nickel sized hail, heavy rain
5 August 2012	Horburg, Eckville	Nickel to quarter sized hail, heavy rain
12 August 2012	Calgary, Cochrane, Water Valley	Golf ball sized hail

2.2 WRF model

The Weather Research and Forecasting (WRF) model is the NWP model chosen for this study. The WRF model was developed at NCAR through partnership with the National Oceanic and Atmospheric Administration (NOAA) and several other organizations and universities including the Air Force Weather Agency and the University of Oklahoma. Because of this diverse partnership, the WRF model has the efficiency and flexibility to effectively serve both the academic community and forecast operations. It is a full physics model with state-of-the-art portable code making it

capable of running effectively on many different computer architectures (Michalakes et al. 1999, Skamarock et al. 2008).

The Environmental Modeling System (EMS) software package (WRF-EMS) (Rozumalski 2006) was developed to encourage the use of the WRF model within U.S. National Weather Service (NWS) forecast offices by simplifying its setup and execution. Several NWS forecast offices are now running high-resolution WRF-EMS simulations locally, with the output being assessed daily by forecasters for many different weather events (Keighton et al. 2009, Zavodsky et al. 2014). This package also makes the model more accessible to researchers. Tota et al. (2014) assessed the accuracy of surface air temperatures and precipitation patterns produced by WRF-EMS over Santarém, Brazil, and Flesch and Reuter (2012) used WRF-EMS in an "off-the-shelf" manner to demonstrate the proficiency of the WRF model for forecasting flooding events in Alberta. This thesis also uses WRF-EMS 3.1 in an "off-the-shelf" manner. This gives us the ability to easily configure and execute the model and allows us to assess the model's accuracy with default settings.

The WRF model domain for this study covers a large portion of western Canada with a 12 km resolution grid, and has a nested 4 km resolution grid covering Alberta (Figure 2-2). Information is exchanged between the outer and inner domains during model runs. This two-way nesting configuration decreases computational expense as it allows for high-resolution computations only over the area of interest instead of over the entire primary domain of western Canada (Gill and Pyle 2012). The model output used in this study is from the inner domain.

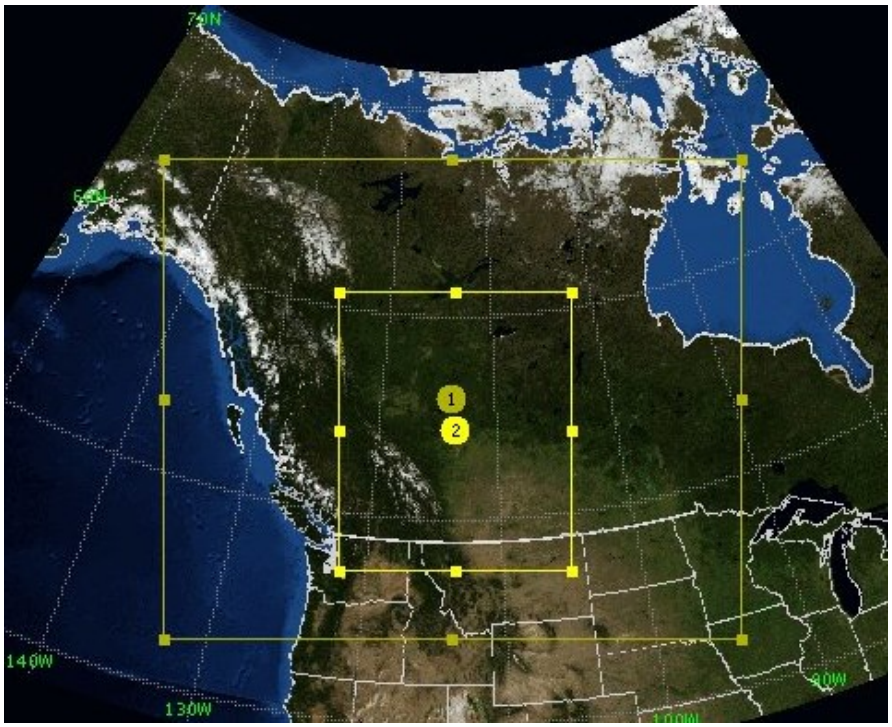

Figure 2-2. WRF model domain setup for this study, with a parent domain (larger rectangle) and a nested child domain over western Canada. The center of each domain is indicated by the yellow circle, where the number refers to the domain. The parent grid is domain 1 and the nested grid is domain 2.

The parent domain uses a Kain-Fritsch cumulus parameterization scheme while the inner domain has a resolution that is sufficient to simulate convection explicitly. This allows for a more realistic treatment of the physics of convection within the high-resolution domain (Done et al. 2004). The Kain-Fritsch scheme was chosen for the outer grid because it has shown more skill for predicting warm season precipitation compared to other schemes (Wang and Seaman 1997, Pennelly 2013). It also has greater forecast accuracy of surface weather features such as temperature gradients, wind shifts, and mesolows, which are critical for triggering thunderstorm development on the Prairies (Wang and Seaman 1997). The Kain-Fritsch scheme was specifically designed for mesoscale applications, and its convective forecast skill may be attributed to its inclusion of parameterized moist downdrafts, as well as its convective available potential energy (CAPE)-based closure assumption, where convection is triggered by the amount of CAPE at a grid point (Kain 2004, Wang and Seaman 1997). In addition, the

Advanced Research WRF (ARW) dynamic core, developed and supported by NCAR, was chosen over the Nonhydrostatic Mesoscale Model (NMM) core for this study because the ARW core has shown more skill for predicting convective initiation and precipitation in the warm season (Jong-Chul et al. 2007, Watson et al. 2007). Table 2-2 contains a summary of the WRF model configuration used for this study.

Table 2-2. A summary of the WRF model configuration used for this study.

Characteristic	**WRF model**
Horizontal grid spacing	Nest: 4 km Parent domain: 12 km
Dynamic core	Advanced Research WRF (ARW), Non-hydrostatic
Data set for initial and boundary conditions	North American Regional Reanalysis (NARR)
Cumulus parameterization scheme	Nest: none Parent domain: Kain-Fritsch (Kain 2004, Kain and Fritsch 1990, 1993)
Microphysics scheme	Lin et al. (1983)
Planetary boundary layer scheme	Yonsei University (Hong et al. 2006)
Land surface physics scheme	Noah (Chen and Dudia 2001)
Projection	Lambert Conformal
Initialization time	0600 UTC
Simulation length	30 hours

The WRF model was initiated at 0600 UTC for each storm day in Table 2-1. Output model Gridded Binary (GRIB) files containing simulated radar reflectivity (dBZ) values over the nested domain were then obtained from 1200 UTC until 1200 UTC the following day, after 6 hours of model spin-up time. The frequency of the output files was every 10 minutes, to match the frequency of the radar data. Shapefiles containing the desired dBZ values at 750 mb were then generated from the model GRIB files to facilitate the process of thunderstorm track selection using ArcMap (Esri ArcGIS 10.0). Model dBZ values at 750 mb are used for this study because they are close to the average pressure level of a CAPPI 1.5 km radar product over Alberta.

The model storm track generation and selection process is similar to that for the radar data. One important change is the use of different input values for the Inverse Distance Weighting (IDW) interpolation technique in ArcMap to account for differences in coordinate system and grid point spacing between the model and radar data. IDW interpolation was used to contour both the model and radar data because the grid points were generally closely spaced, and negative dBZ values and excessive smoothing were not desired. This technique allows for a weight to be supplied during the interpolation, specifying how much influence the closest data points have on the result, as well as the number of points to use in the averaging. This allows for greater control of the interpolation process and higher comparability of the results from both the model and radar grids despite their differences.

There are also a few additional track selection criteria to fulfill for the model data due to its increased spatial and temporal availability. This allows the selected model and radar tracks to remain comparable to each other. Qualifying model tracks must have initiated within 200 km from any of the radar tracks on a storm day. This distance threshold was chosen because of its general acceptance as the maximum distance that an atmospheric sounding can be from a location and remain representative of the air mass (Dupilka & Reuter 2006). There is also the requirement that each model track must have initiated within 3 hours before or after the radar tracks of the storm day. This keeps the radar and model storm tracks temporally comparable. The following list gives the storm track selection criteria for the model data.

Model storm track selection criteria

Each model storm track must

- be produced by a storm cell with a 35 dBZ area greater than 10 km^2 and having its center at the dBZ weighted mean center,
- start within Alberta and remain within Canadian radar coverage,
- initiate within 200 km from any of the selected radar storm tracks on the storm day,

- last for at least 6 consecutive model output files (50 minutes),
- not be missing a 35 dBZ weighted mean center for more than 1 consecutive model output file (more than 10 minutes) along the length of the track (this could occur if the 35 dBZ area is too small or non-existent),
- end before the last radar scan gathered for the storm day,
- initiate within (or exactly) 3 hours before the initiation of the first radar storm of the storm day or must have initiated within (or exactly) 3 hours after the initiation of the last radar storm of the storm day, and
- end at the time step before the first scan where the 35 dBZ area is greater than 576 km^2. If this area threshold is reached before the track has met the minimum duration threshold, the track is discarded.

The following procedures are used for storm splits and merges.

- If a storm cell splits into two cells, two tracks are created that share the initial merged part of the track; however, for a track to be included, the second part of the track must last at least 5 consecutive model output files (40 minutes) and not be missing more than 1 consecutive output file (more than 10 minutes) along its length.
- If two storms merge into one cell, the two tracks continue and share the merged part of the track; however, for the tracks to be included, the second part of the track must last at least 5 consecutive model output files (40 minutes) and not be missing more than 1 consecutive output file (more than 10 minutes) along its length.

Chapter 3

Case Study: Calgary Hailstorm of 12 August 2012

Severe weather outbreaks in Alberta are often caused by strong surface heating along the foothills ahead of an advancing trough. This promotes moist air advection from the Prairies and upslope flow, which supports the initiation of convection in the presence of cooling air aloft and strong southwesterly mid-level winds (Smith and Yau 1993). The storm day dynamics of the Calgary hailstorm on 12 August 2012 were similar to this classic storm setup and all of the ingredients were present for devastating storms to develop. Conditions through southern Alberta on the morning of 12 August 2012 were cloudy and humid following the previous day's storm activity. An eastward-moving surface trough in western British Columbia and an approaching surface low in Idaho promoted continued instability and cloud development along the Rocky Mountains ahead of these features. As the day progressed, the atmosphere destabilized as the air cooled slightly aloft and diurnal heating warmed the surface, while high surface humidity was maintained by southeasterly upslope flow against the Rockies. The formation of a vorticity center over southern Alberta in the afternoon was the likely trigger for severe storms given these favorable conditions.

Back to back hailstorms pounded Calgary on the 12th and 14th of August 2012 resulting in a combined $552 million in insured damages and placing the combined event in the top ten worst natural disasters in Canadian history (Western Direct Insurance 2014). This chapter gives a brief overview of the hailstorm of 12 August to emphasize the potential severity of storms on the Prairies and the importance of timely and accurate thunderstorm forecasts. It also illustrates the storm track selection process and the comparison done between the radar and model tracks in this thesis. It should give a better understanding of the data and procedures used to generate the results outlined in the subsequent chapters.

For this study, the storm "day" of 12 August 2012 begins at 1200 UTC (6:00 am MDT) 12 August 2012 and ends at 1200 UTC (6:00 am MDT) 13 August 2012. CAPPI 1.5

km radar data from the Strathmore and Schuler radars in southern Alberta was obtained and analyzed for radar storm tracks using the criteria outlined in section 2.1. Simulated radar reflectivity fields from the WRF model were also generated and analyzed for model storm tracks as outlined in section 2.2. After completion of this analysis and the track selection process, there were 3 model storm tracks and 10 radar storm tracks created for this day. These tracks and their characteristics are given in Table 3-1 and Table 3-2, respectively. Figure 3-1 shows these tracks on a map of southern Alberta.

Table 3-1. The model storm tracks on 12 August 2012 and their characteristics.

Start Time and Date (UTC)	**Start Latitude (°N)**	**Start Longitude (°W)**	**Length (km)**	**Duration (min)**	**Speed (km/h)**	**Mean Direction (°)**	**Maximum Intensity (dBZ)**
22:50 12 August 2012	50.66	114.62	109.1	210	31.2	291.5	51.0
08:10 13 August 2012	51.39	111.28	87.1	120	43.6	288.5	45.0
08:30 13 August 2012	51.58	111.35	55.7	70	47.7	289.2	43.0

Table 3-2. The radar storm tracks on 12 August 2012 and their characteristics.

Start Time and Date (UTC)	Start Latitude (°N)	Start Longitude (°W)	Length (km)	Duration (min)	Speed (km/h)	Mean Direction (°)	Maximum Intensity (dBZ)
21:20 12 August 2012	52.10	115.59	178.1	470	22.7	316.5	66.5
21:40 12 August 2012	50.16	114.37	130.2	380	20.6	290.0	69.0
04:30 13 August 2012	49.56	112.79	158.4	300	31.7	278.2	60.5
04:30 13 August 2012	49.56	112.79	105.1	240	26.3	283.5	60.5
04:30 13 August 2012	49.56	112.79	141.0	330	25.6	279.6	64.0
06:00 13 August 2012	49.73	111.72	117.9	220	32.2	286.2	61.0
06:00 13 August 2012	49.73	111.72	98.1	160	36.8	264.3	61.0
06:00 13 August 2012	49.35	111.14	120.5	240	30.1	279.2	64.0
09:10 13 August 2012	49.44	111.81	25.0	50	30.0	271.0	53.5
09:30 13 August 2012	49.82	112.08	57.6	60	57.6	269.6	58.5

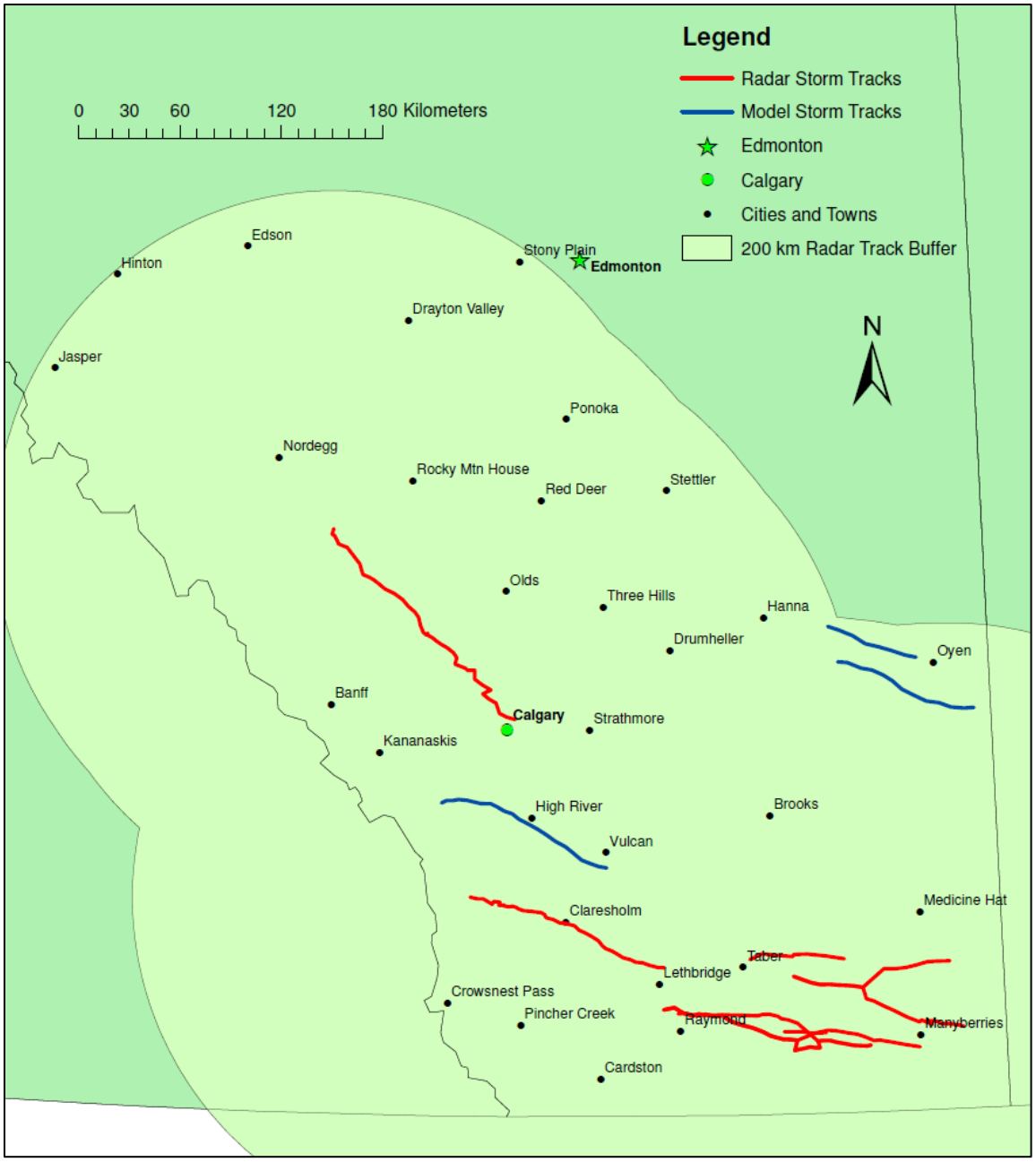

Figure 3-1. Model (blue) and radar (red) storm tracks on 12 August 2012 over southern Alberta. The light green area is a 200 km buffer zone around the radar tracks. Each model track must have initiated within this zone.

The storm cell that hit Calgary was the first of the day to reach an intensity of 35 dBZ, the intensity threshold for a severe thunderstorm in this study. This occurred at 2120 UTC about 53 km southeast of Nordegg and 55 km southwest of Rocky Mountain House along the Alberta foothills. The storm then intensified and tracked southeast

towards the community of Water Valley. Residents of this community reported loonie sized hail (27 mm in diameter) to Environment Canada at 0215 UTC. The storm then moved into Calgary and began dumping golf ball sized hail (45 mm in diameter) on northern sections of the city at 0400 UTC 13 August 2012 (10:00 pm MDT 12 August 2012) and causing record damage. Toonie sized hail (29 mm in diameter) was also reported by a pilot on the ground at the Calgary airport at 0434 UTC.

The first WRF model storm of the day reached 35 dBZ at 2250 UTC about 65 km southwest of Calgary and then headed southeast, passing the towns of High River and Vulcan before weakening. The starting point of this corresponding model storm track is about 174 km south-southeast of the start of the Calgary storm track. Figure 3-2 shows the evolution of the Calgary hailstorm, the first storm to reach 35 dBZ on 12 August 2012, along with the first storm of the day produced by the WRF model.

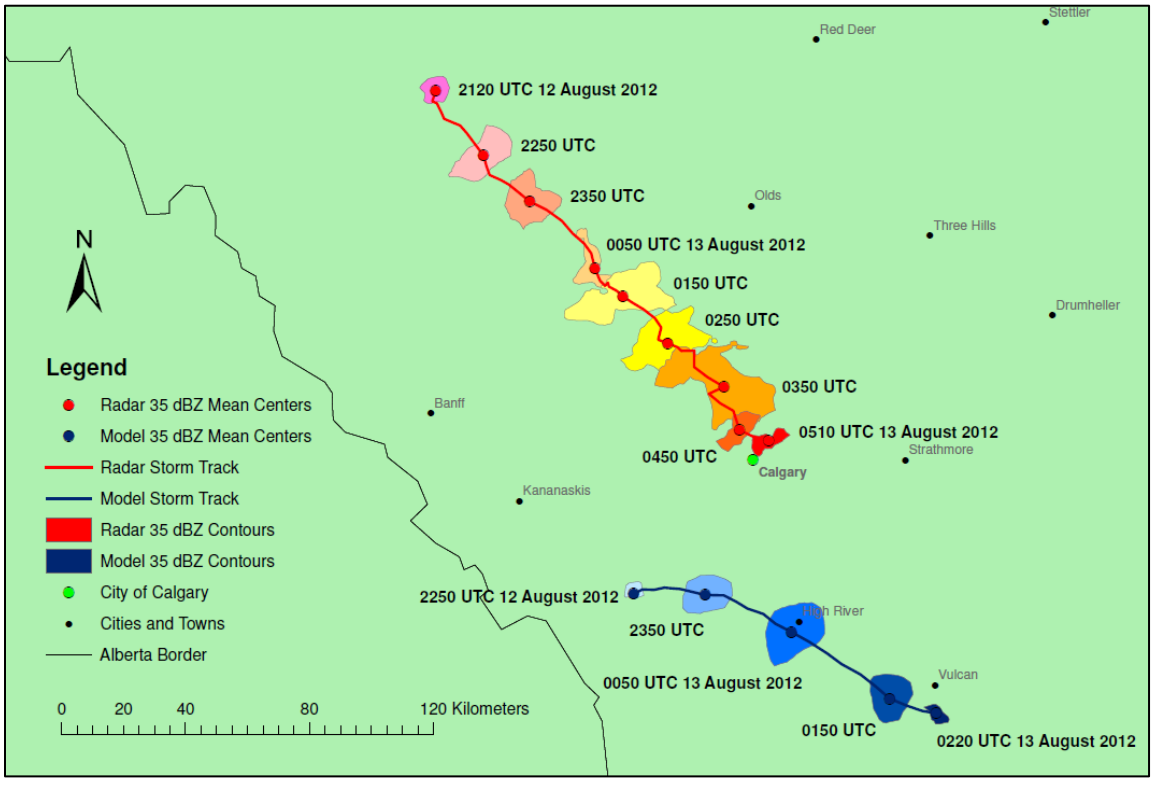

Figure 3-2. Storm tracks of the Calgary hailstorm and the first model storm on 12 August 2012, along with selected 35 dBZ contours and their dBZ weighted mean centers.

A mean direction vector for each storm track was calculated after completion of the storm track selection process. The vectors of the storm tracks for 12 August 2012 are given in Figure 3-3. For consistency during the comparison of simulated and observed tracks, each track direction value is taken to be the direction from where a storm comes from, and is therefore opposite to the mean direction given by each vector. The speed of each storm was obtained by dividing the storm track length, not the vector length, by the storm's duration.

The set of radar storm tracks for this day includes two storm splits and one storm merge, with the merge occurring between a previously split cell and another storm cell. The track of the cell that passed over Calgary also split just before reaching the city, but the second track did not qualify because the size of the 35 dBZ contour quickly exceeded the area threshold of 576 km^2. An evolution of the Calgary storm cell and its track are given in Figure 3-4, with the 35 dBZ contours of the second cell very evident.

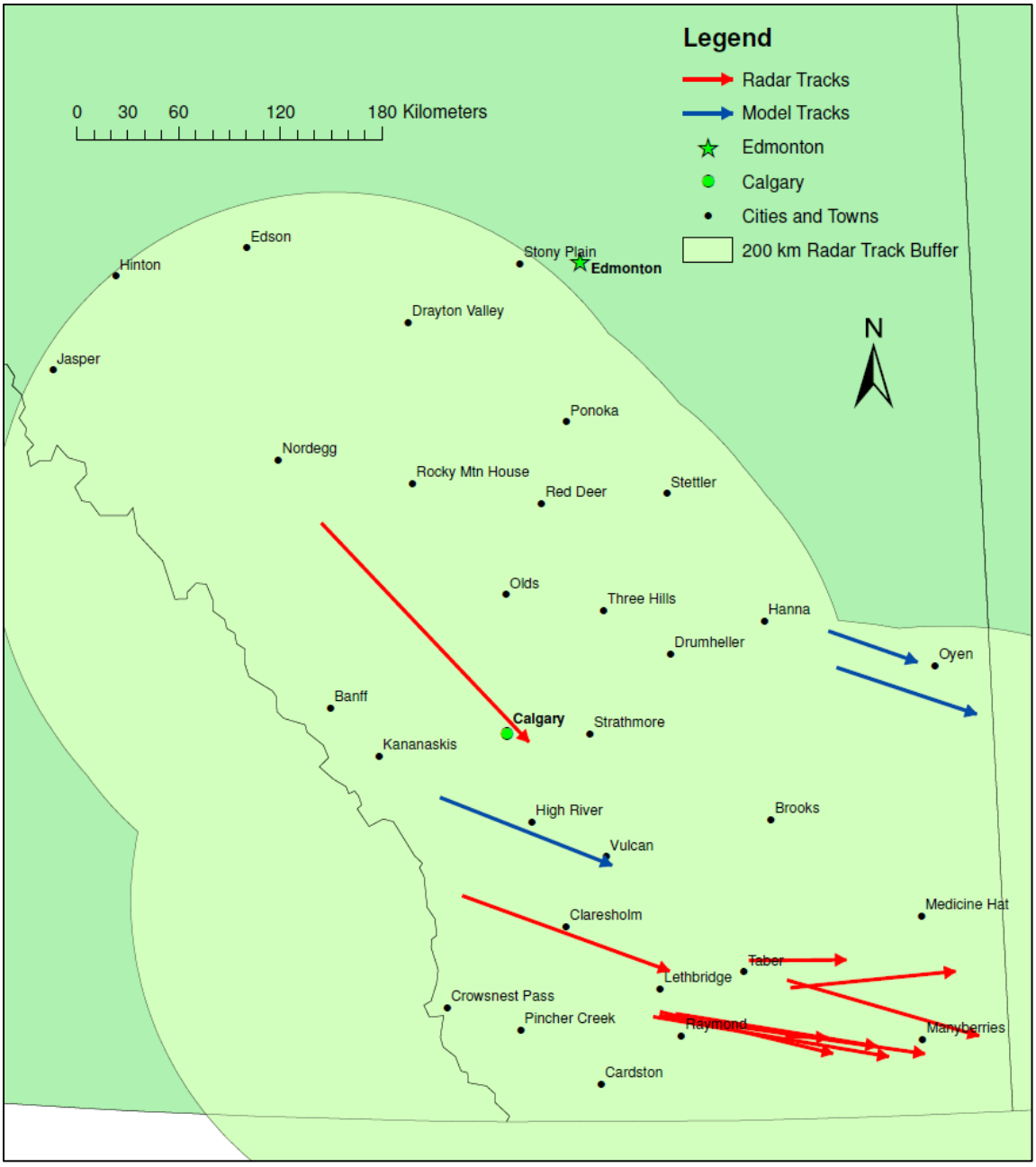

Figure 3-3. Model (blue) and radar (red) mean direction vectors of the storm tracks on 12 August 2012 over southern Alberta. The light green area is a 200 km buffer zone around the radar tracks. Each model track must have initiated within this zone.

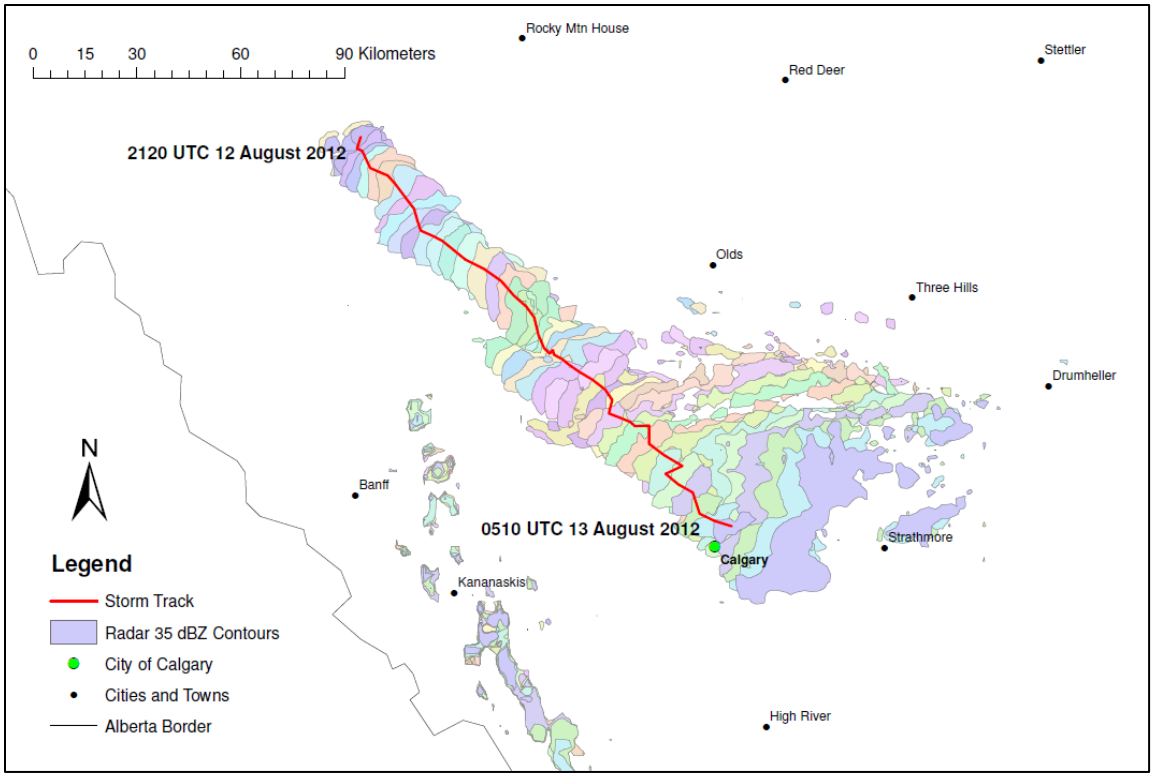

Figure 3-4. Storm track and radar 35 dBZ contours of the Calgary hailstorm on 12 August 2012. A different color is used to distinguish the 35 dBZ contours at each 10 minute time step along the track. The storm cell split just before reaching Calgary, but the second (largest) cell's track did not qualify for this study because the size of its 35 dBZ contour quickly exceeded the area threshold.

The first and most simple criterion that had to be met by each storm track was its origin within Alberta. No tracks in this study originated beyond Alberta's borders and crossed into the province. This allows for a comparison of storm initiation along with storm motion, and the primary location of storm initiation in Alberta is along the foothills. In the case of 12 August 2012, the first three storms of the day initiated along the foothills and we see that the model and radar storms propagate and continue to initiate farther east with storm start time (Figures 3-1 and 3-3). This can likely be attributed to the motion of the vorticity center through southern Alberta and the development of storms ahead of it as it traveled southeast.

The time of day in which storms reach 35 dBZ seems to affect the properties of the storm tracks. Track duration, length, and maximum intensity (dBZ) all decrease with

track start time on 12 August 2012 (Figures 3-5, 3-6, and 3-7). This means that storms initiating later in the day did not travel as far, last as long, or become as intense as storms that initiated earlier in the day. It is possible that these changes are due to decreasingly favorable storm conditions, such as surface heating and upslope flow, as the day progressed into the evening hours.

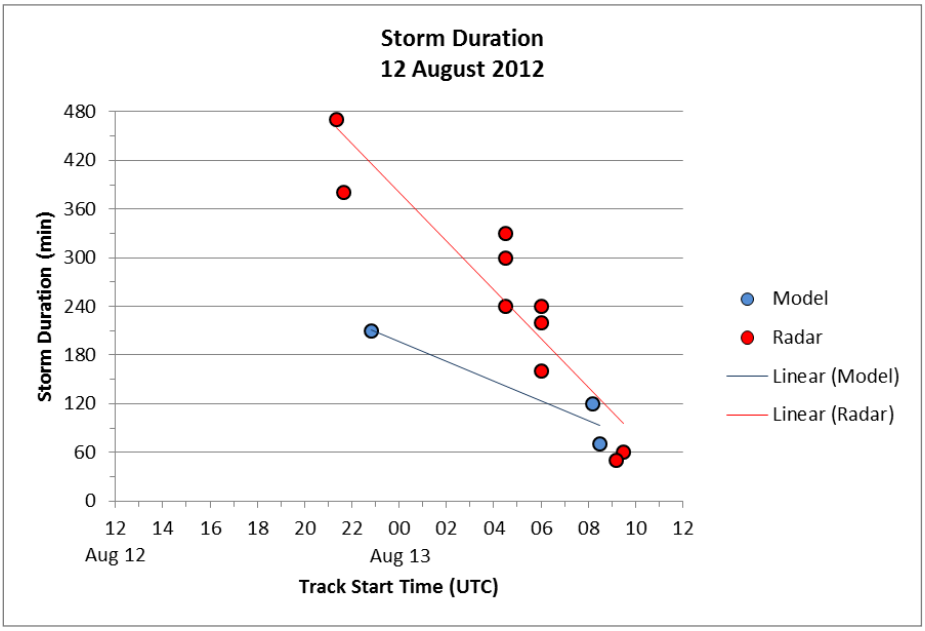

Figure 3-5. Duration (min) of the model and radar storms on 12 August 2012.

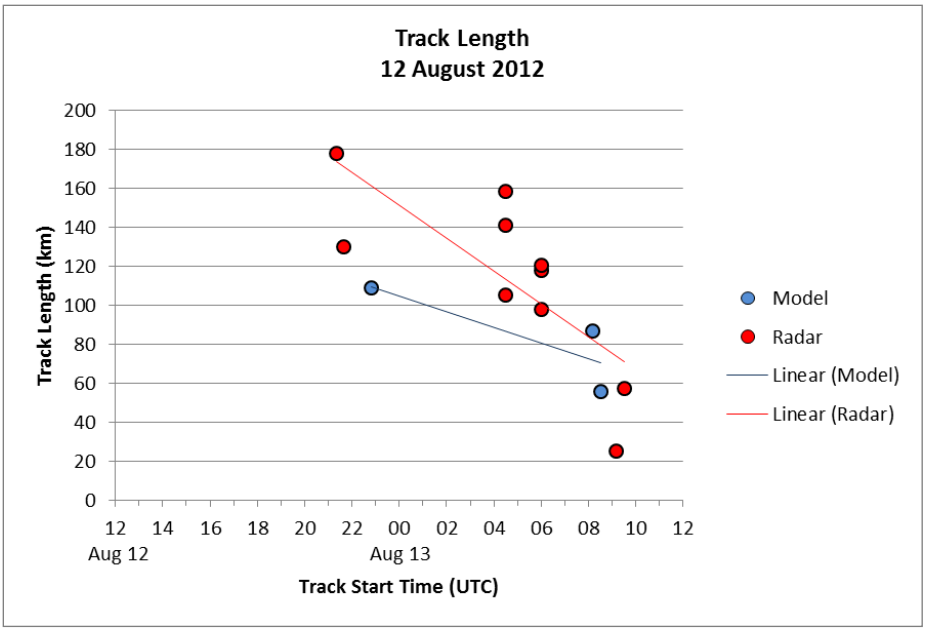

Figure 3-6. Length (km) of the model and radar tracks on 12 August 2012.

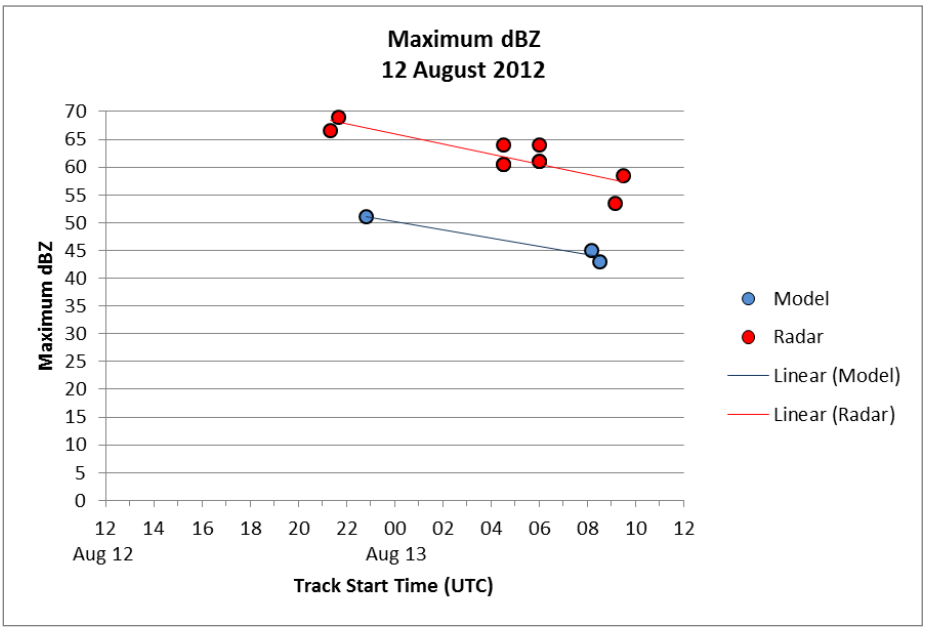

Figure 3-7. Maximum dBZ values reached by the model and radar storms on 12 August 2012.

In the case of 12 August 2012, we find that storms that are more intense (have higher maximum dBZ values) tend to travel at slower speeds (Figure 3-8). Figure 3-8 also shows the difference in intensity between the storms, with the radar-observed storms

being more intense than those produced by the WRF model. A more in-depth investigation into these characteristics and relationships, as well as additional analysis for all storm days, is given in chapter 4.

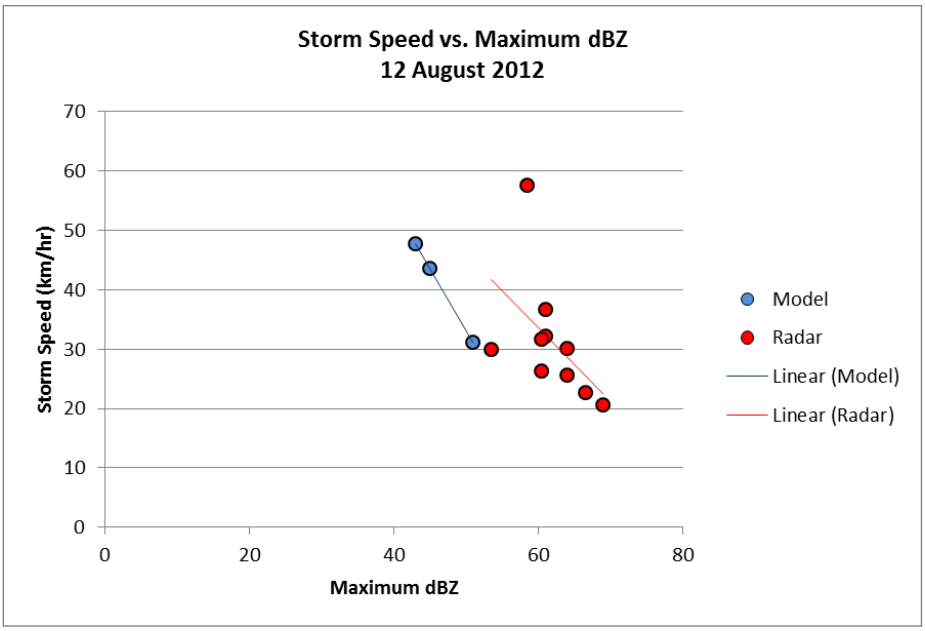

Figure 3-8. Relationship between speed (km/hr) and maximum dBZ value for the model and radar storms on 12 August 2012.

Figure 3-9 shows the 0000 UTC atmospheric sounding from Stony Plain, Alberta (WSE) on 13 August 2012. This sounding is the closest sounding to the Calgary hailstorm, both spatially and temporally, and is the sounding that best represents the atmospheric conditions during the storm. Figure 3-10 is the associated hodograph for this sounding. A hodograph displays the wind speed and direction through the atmosphere, with the distance of each point from the origin representing the magnitude of the wind at that level. The location of each point within the diagram represents the direction that the wind is traveling towards with respect to the origin.

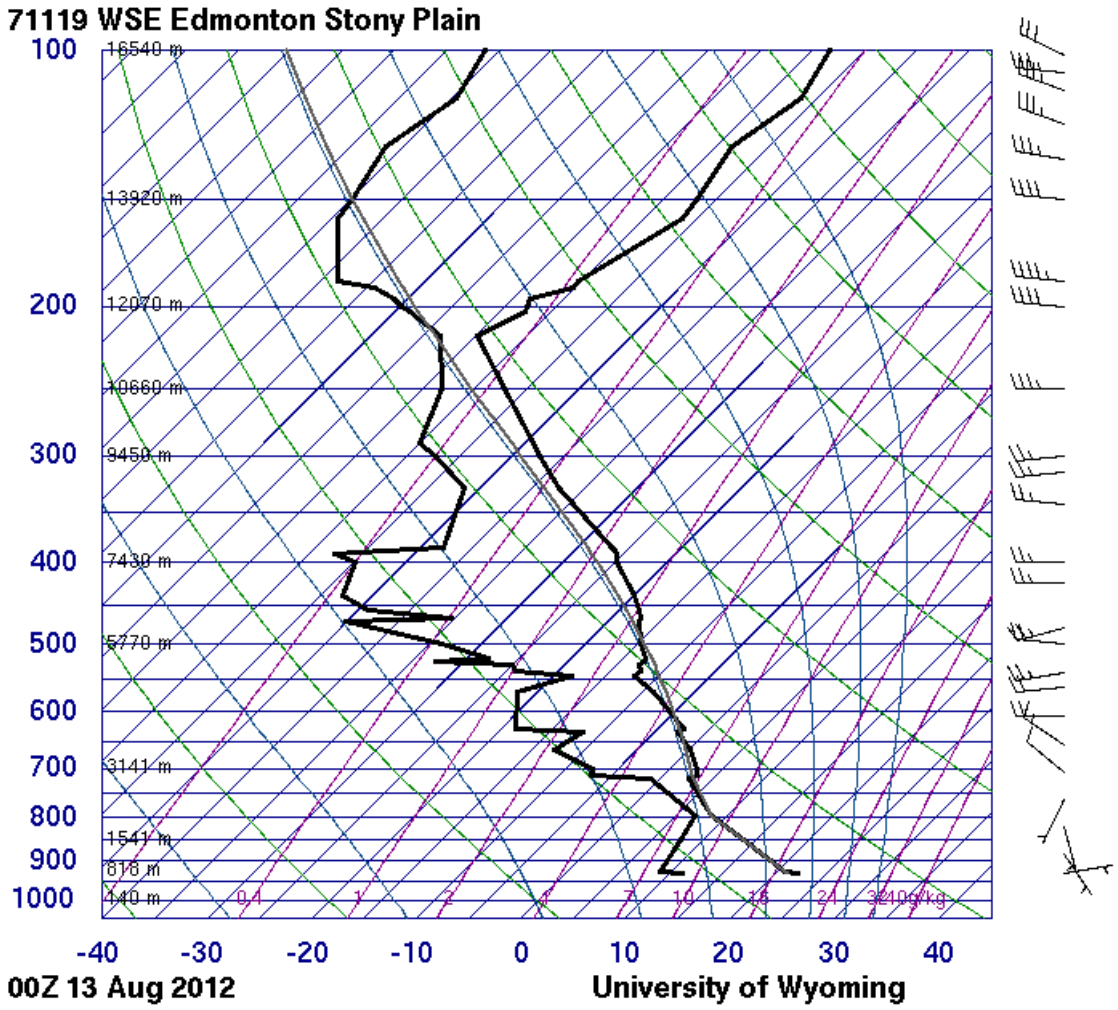

Figure 3-9. 0000 UTC atmospheric sounding from Stony Plain, Alberta (WSE) on 13 August 2012. The wind at each standard pressure level is represented by a wind barb to the right of the Skew-T diagram.

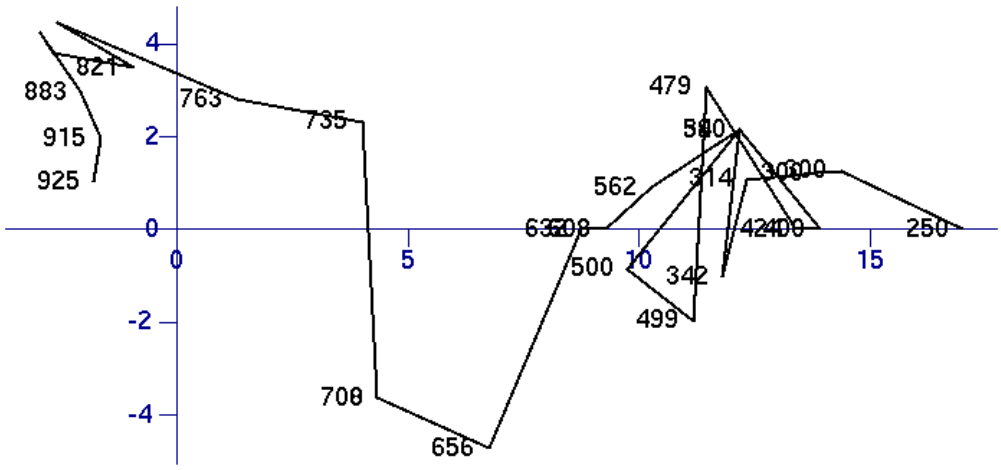

Figure 3-10. 0000 UTC hodograph from Stony Plain, Alberta (WSE) on 13 August 2012.

Mean wind can be calculated from an atmospheric sounding or hodograph following the procedure outlined in Appendix B. For the 0000 UTC sounding from Stony Plain on 13 August 2012 (Figures 3-9 and 3-10) the 0-6 km mean wind is calculated to have a magnitude of 22 km/hr and a direction of 262°. From this value we can calculate the forecast storm speed and direction using the Traditional Method, which is given as 30° to the right and 75% of the magnitude of the mean wind. More information on the Traditional Method is given in chapter 5. The forecast storm motion given by the Traditional Method is 17 km/hr from a direction of 292°. Bunkers Method is another method used to predict the motion of severe storms using a hodograph. The procedure for using Bunkers Method on a hodograph is outlined in Appendix C. The forecast storm motion given by Bunkers Method using the 0000 UTC Stony Plain hodograph (Figure 3-10) is 32 km/hr from a direction of 320°.

The mean speed and direction of the radar-observed storms for 12 August 2012 is 31 km/hr from a direction of 282°. Therefore, Bunkers Method gives the best estimate of storm speed for this day and the Traditional Method gives the best estimate of storm

direction. The mean speed and direction of the WRF model storms on 12 August 2012 is 41 km/hr from a direction of 290°. Therefore, the WRF model gives an even better estimate of storm direction for this day, but the mean speed of the model storms is too fast compared to that of the radar storms, and is faster than the predicted speed from both the Traditional Method and Bunkers Method. A more in-depth comparison between the model and radar tracks is given in chapter 4, and an investigation into the accuracy of the forecast storm motion from the Traditional Method and Bunkers Method for all storm days is made in chapter 5.

Chapter 4

Comparison between Simulated and Observed Tracks

4.1 Storm tracks

This chapter presents the combined results of our comparison between the simulated and observed storm tracks, focussing on storm speed, direction of motion, track length, storm duration, and storm intensity. Any overall trends in the performance of the WRF model are presented, as well as some results from individual storm cases. To be consistent, storm speed is calculated by dividing the storm track length by the storm duration, and storm direction is found by calculating the mean direction of each track and determining the direction from which each storm comes from, following the usual compass convention. Higher direction values refer to storms that move in a more clockwise direction as they travel from west to east, relative to storms with lower direction values.

4.1.1 Speed

Of the 14 storm cases in this study, 10 cases (71%) are found to have the minimum storm speed greater for the model than for the radar storms, and 8 cases (57%) have the maximum storm speed greater for the model than for the radar storms (Figure 4-1). Additionally, the mean and the median of storm speed are greater for the model in 12/14 cases (86%) (Figure 4-1). Therefore, the WRF model generally produces storms which move faster than radar-observed storms. When the track length and duration are plotted for all model and radar storm cells in each case, and the average speed of the cells is calculated using the slope of the graph, it is found that the average storm speed is greater for the model than for the radar storms in 13/14 cases (93%). Figure 4-2 is a summary scatter plot of length versus duration for all of the storm tracks in this study. The slope of the best fit lines for the model and radar data gives the

average model and radar storm speed, respectively. From this figure we see the tendency for WRF model storms to move faster than radar-observed storms.

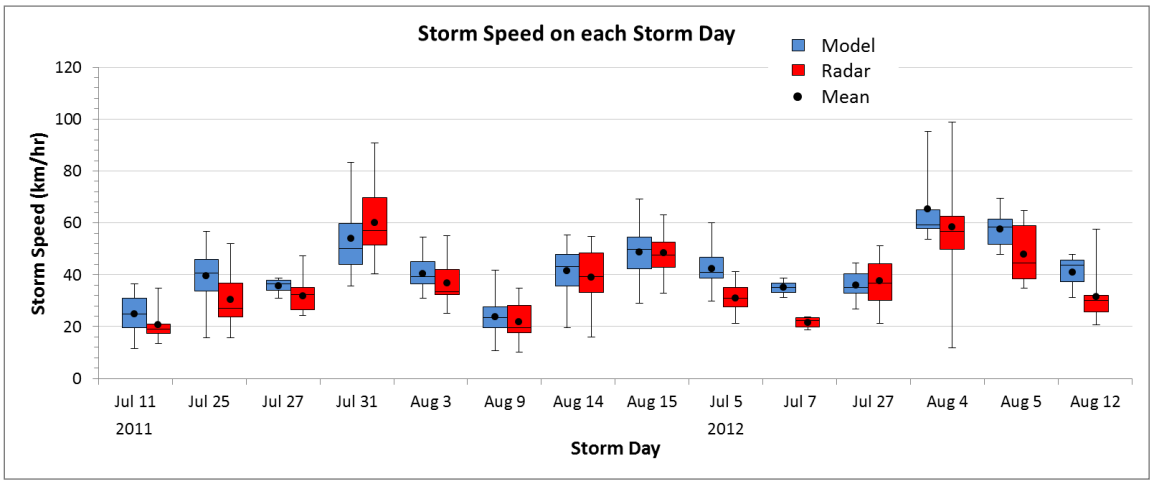

Figure 4-1. Speed (km/hr) of the model and radar storms on each storm day. Box plots show median values (horizontal line), mean values (dot), 50th percentile values (box outline), and minimum and maximum values (whiskers).

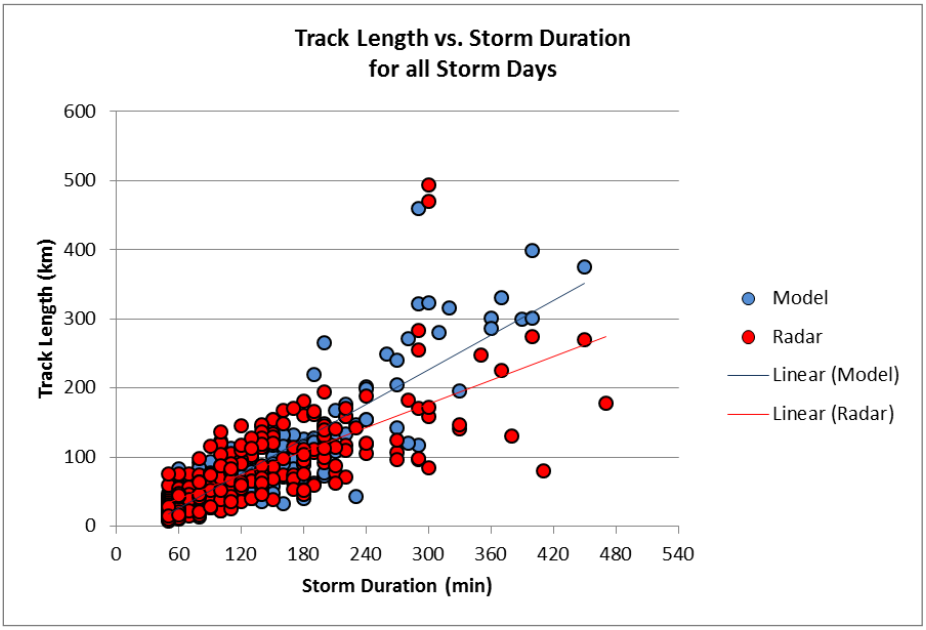

Figure 4-2. Relationship between track length (km) and storm duration (min) for the model and radar storms on all storm days.

From Figure 4-1 we also find that the spread of values between the lowest and highest storm speed is less for the model than for the radar in 8/14 cases (57%), and the storm speed interquartile range is less for the model than for the radar in 9/14 cases (64%). Therefore, the WRF model produces storms with less of a spread of speeds compared to radar-observed storms, especially for the middle 50% of speed values. It is possible that sample size may affect the range of values in each storm case, since there is a tendency for larger sample sizes to have a larger range of values; however, this does not seem to be a major factor in our results for storm speed. The model produced more storm tracks than radar tracks in only 8/14 cases (57%). The storm case with the greatest difference between the number of model and radar tracks, 9 August 2011, had 58 more model tracks (total of 95) than radar tracks (total of 37) but does not exhibit a much larger range of speeds for the model storms than for the radar storms (Figure 4-1). The storm case with the smallest difference between the number of model and radar tracks, 5 July 2012, had 1 more radar track (total of 15) than model track (total of 14) but had a larger spread of speeds for the model tracks than for the radar tracks (Figure 4-1). Therefore, we conclude that the difference in the number of model and radar storm tracks in each case does not dramatically affect the results of our storm speed comparison, though it is possible that this difference may influence the results presented in other sections of this thesis.

When comparing storm speed with the start time of each track, we find that 11/14 cases (79%) have the radar storm speed increasing with track start time, suggesting that faster storms develop later in the storm day; however, it is uncertain whether this relationship holds for the WRF model storms. Only 7/14 cases (50%) have the model storm speed increasing with track start time. Figure 4-3 is an example of one case in which the radar storm speeds tend to increase with time while the model storm speeds do not.

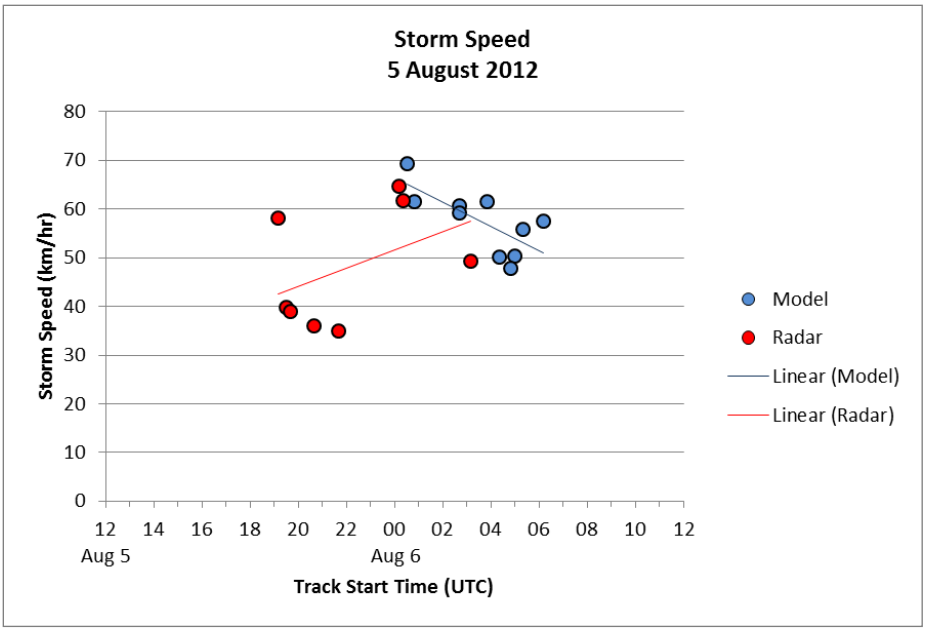

Figure 4-3. Speed (km/hr) of the model and radar storms on 5 August 2012.

4.1.2 Direction

The maximum storm track direction given by the WRF model is less than that of the radar storms in 11/14 cases in this study (79%) while the minimum track direction is less for the model than for the radar storms in 7/14 cases (50%) (Figure 4-4). Also, the mean and median of track direction is less for the model than for the radar storms in 11/14 cases (79%) and 12/14 cases (86%), respectively (Figure 4-4). This shows that the model produces storms that move in a more counter clockwise direction, or are possibly less right-moving, than radar-observed storms. Right-moving storms are those that turn to the right as they propagate, usually developing in environments with strong wind shear in the 0-6 km layer. These cells are often more severe in nature, becoming supercells with a strong rotating updraft, and tend to last longer and travel farther than non-severe thunderstorms (Bunkers et al. 2000).

Figure 4-4 also shows that the spread of track direction between the lowest and highest value is less for the model than for the radar storms in 12/14 cases (86%), and the track direction interquartile range is less for the model than for the radar in 11/14

cases (79%). Therefore, the WRF model produces storms with less of a spread of storm track direction values than radar-observed storms.

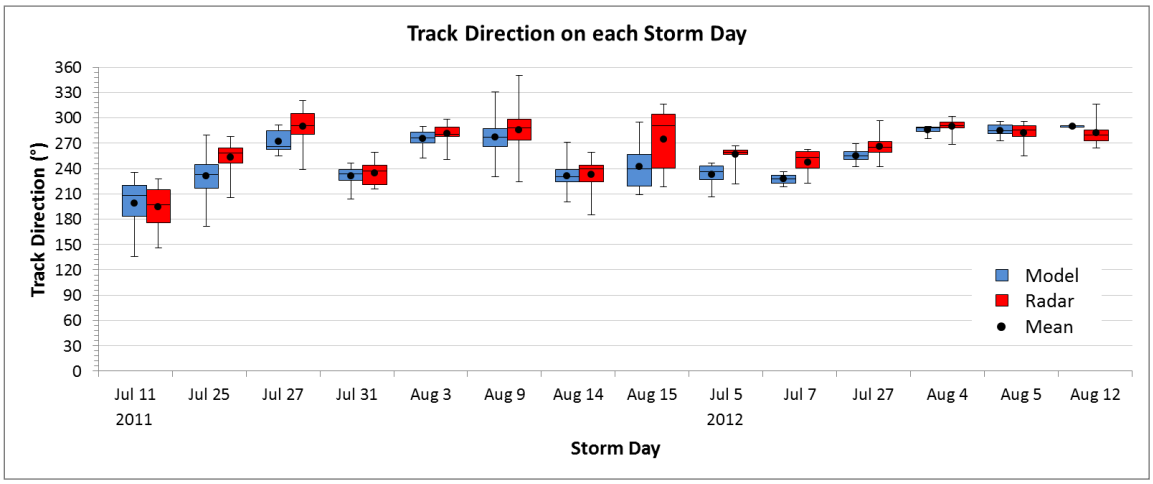

Figure 4-4. Direction (°) of the model and radar tracks on each storm day. Box plots show median values (horizontal line), mean values (dot), 50th percentile values (box outline), and minimum and maximum values (whiskers).

Previous research suggests that more intense storms have tracks that are more clockwise, or are more right-moving (Bunkers et al. 2000). To investigate this hypothesis the storm cases in this study were sorted by the maximum dBZ value that was reached by any storm on radar during that storm day. The results are presented in Figure 4-5. Four of the five storm days with the least amount of spread in track direction also have the highest maximum dBZ values, and these storms have some of the highest values for mean, median, minimum, and maximum track direction. This suggests that there is a relationship between track direction and maximum dBZ such that storm days with cells of very high dBZ value also have tracks that are more clockwise, or are possibly more right-moving.

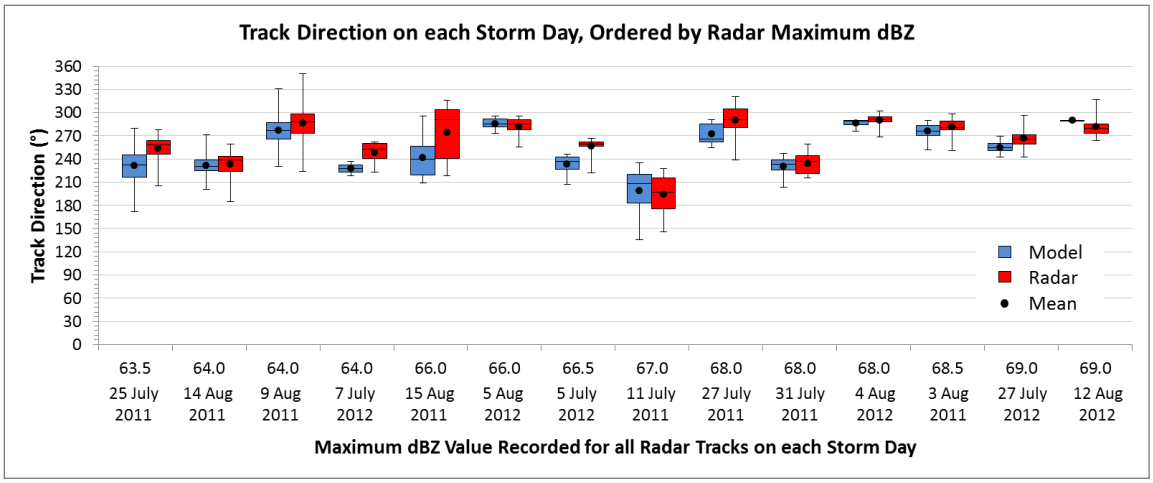

Figure 4-5. Direction (°) of the model and radar tracks on each storm day, ordered by the maximum dBZ value reached by the radar storms. Box plots show median values (horizontal line), mean values (dot), 50th percentile values (box outline), and minimum and maximum values (whiskers).

Scatter plots of maximum dBZ versus track direction for all storm cells were also created for each storm day. Two of these scatter plots are given as examples in Figures 4-6 and 4-7. Model and radar track direction tends to increase (become more clockwise) with increasing maximum dBZ value in 10/14 cases (71%) in this study. The storm cases in Figures 4-6 and 4-7 both demonstrate this tendency. This further supports the existence of a relationship between storm track direction and dBZ value.

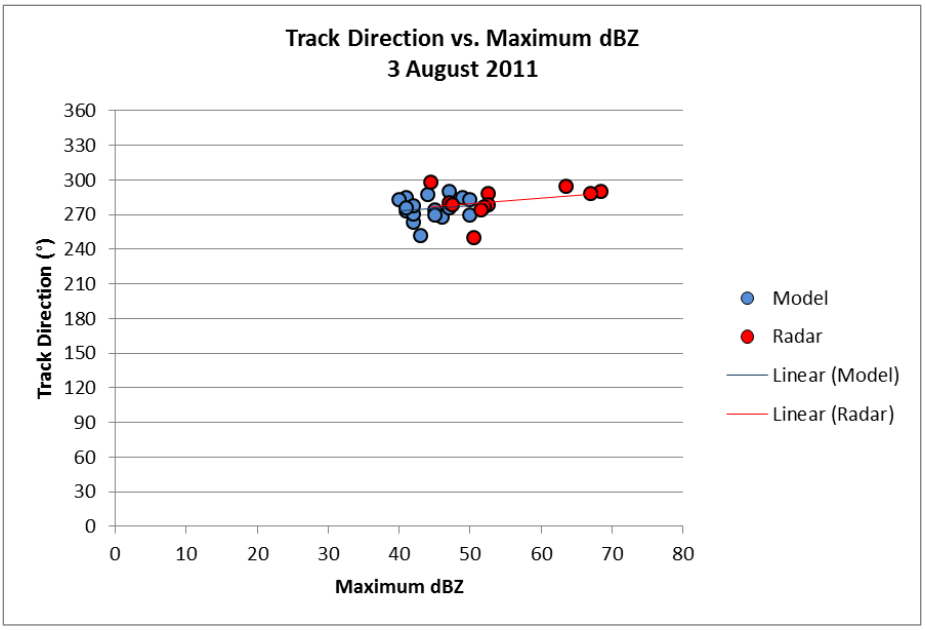

Figure 4-6. Relationship between track direction (°) and maximum dBZ for the model and radar storms on 3 August 2011.

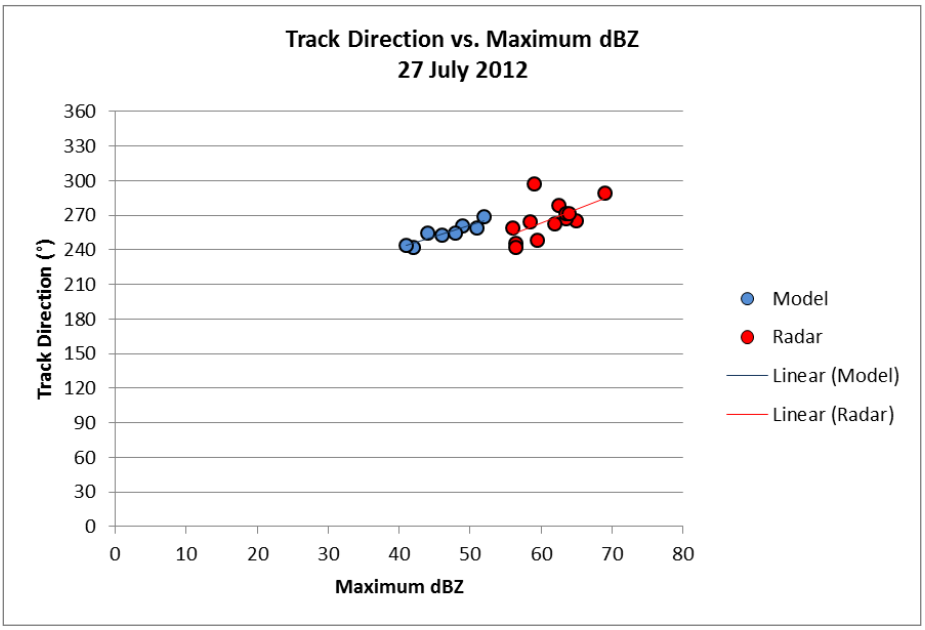

Figure 4-7. Relationship between track direction (°) and maximum dBZ for the model and radar storms on 27 July 2012.

Analysis was done to look for relationships between track direction and storm speed, duration, track length, and track start time. No relationship is found between track direction and storm speed for the WRF model storms, but we find that radar storm speed decreases with increasing track direction in 10/14 cases (71%). This suggests that storms with more clockwise tracks, or possibly more right-moving storms, have slower speeds, though the WRF model did not replicate this trend. It is also unclear whether there is a relationship between track direction and track start time for either the model or radar storms. Therefore, it is unclear from this study whether storms with more clockwise tracks, or storms that are possibly more right-moving, tend to develop earlier or later in the day.

When comparing track direction with track length and duration, we find that track length increases with track direction for both the model and radar storms in 11/14 cases (79%) and 12/14 cases (86%), respectively, while storm duration increases with track direction in 11/14 cases (79%) and 13/14 cases (93%), respectively. This suggests that storms with more clockwise tracks tend to last longer and travel farther, agreeing with Bunkers et al. (2000). It is interesting to note that this relationship holds for the radar storms despite the finding that radar storm speeds tend to decrease with increasing track direction. Therefore, the increase in track length for these storms is due to an increase in storm duration and not an increase in storm speed.

4.1.3 Length

Of the 14 cases in this study, 10 (71%) are found to have the minimum track length greater for the model than for the radar storms, and 9 (64%) have the maximum track length greater for the model than for the radar storms (Figure 4-8). Also, the mean and median of track length are greater for the model in 9/14 cases (64%) each (Figure 4-8). Therefore, the WRF model tends to produce storms with longer track lengths than radar-observed storms. In section 4.1.1 of this thesis we found that the model storms tend to move faster than the radar storms, and this may play a role in why the model

storms also tend to have longer tracks. Due to their higher speeds, the model storms can travel farther than the radar storms in the same amount of time; however, before coming to a conclusion, storm duration is investigated in more detail in section 4.1.4.

It is also found that the spread of track length between the lowest and highest value is greater for the model than for the radar in 8/14 cases (57%), and the interquartile range is greater for the model than for the radar in 10/14 cases (71%) (Figure 4-8). Therefore, the model produces storms with a larger spread of track length compared to radar-observed storms.

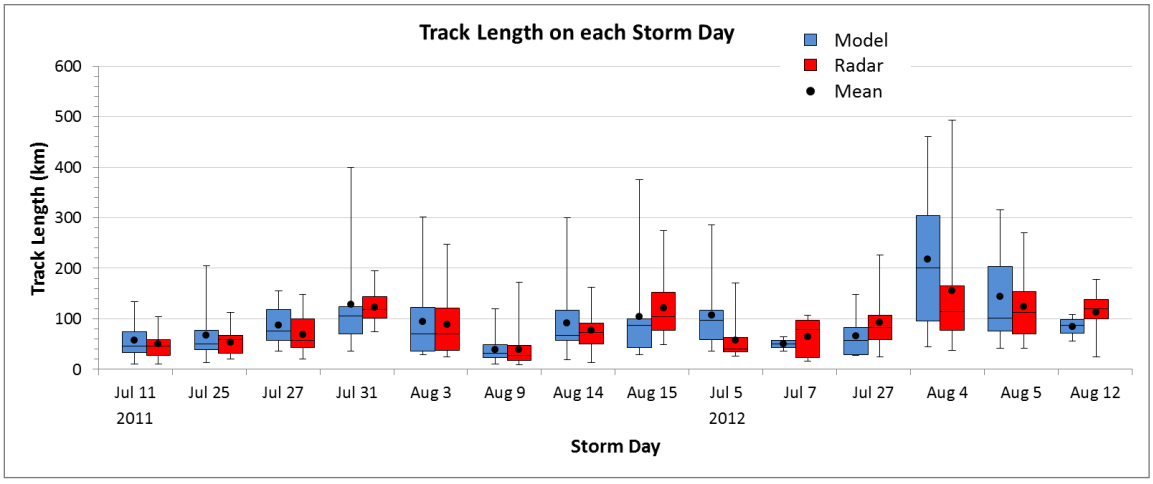

Figure 4-8. Length (km) of the model and radar tracks on each storm day. Box plots show median values (horizontal line), mean values (dot), 50th percentile values (box outline), and minimum and maximum values (whiskers).

In order to investigate any relationship between track length and track start time, scatter plots of these values were created for all storms on each storm day. We find that model and radar track length decreases with increasing track start time in 10/14 cases (71%) and 13/14 cases (93%), respectively. Therefore, storm track length tends to decrease as storms initiate later in the storm day. Figures 4-9 and 4-10 show two storm days, 25 July 2011 and 15 August 2011, that exhibit this relationship for both the model and radar storms.

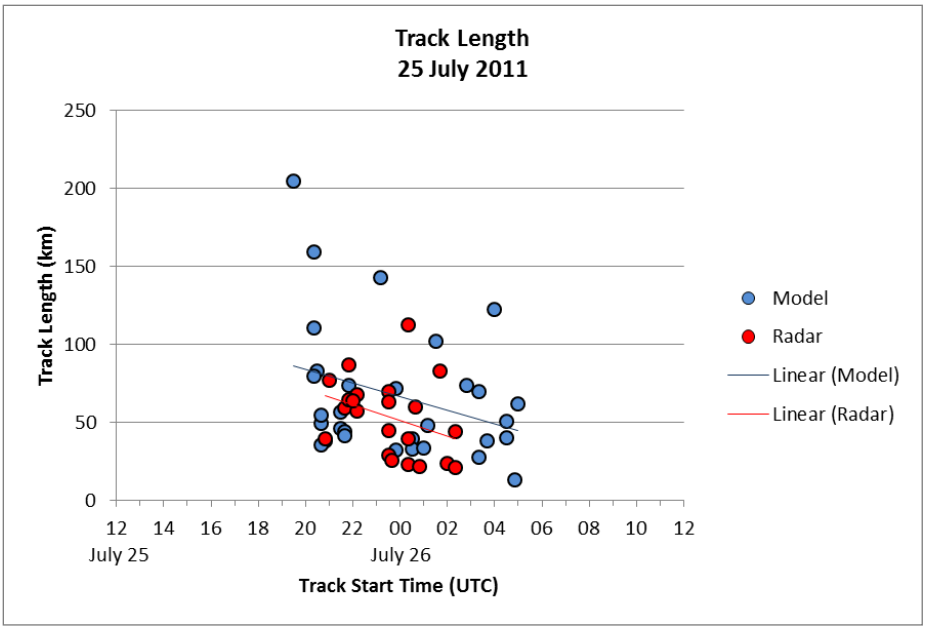

Figure 4-9. Length (km) of the model and radar tracks on 25 July 2011.

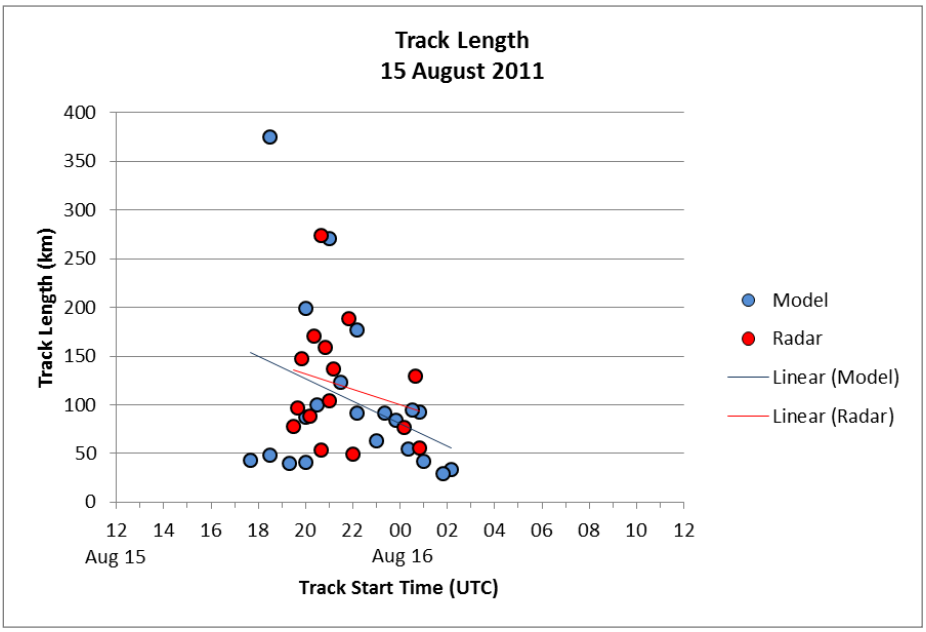

Figure 4-10. Length (km) of the model and radar tracks on 15 August 2011.

4.1.4 Duration

Of the 14 cases in this study, the maximum, mean, and median of storm duration is found to be less for the model than for the radar storms in 8 cases (57%), 9 cases (64%), and 7 cases (50%), respectively (Figure 4-11). Also, the difference in storm duration between the lowest and highest value is less for the model than for the radar in 8/14 cases (57%), and the storm duration interquartile range is less for the model than for the radar in 9/14 cases (64%) (Figure 4-11). Therefore, storms produced by the WRF model have a slightly shorter lifespan and a slightly smaller spread of storm duration than radar-observed storms; however, this difference is marginal. Thus we can conclude that the tendency for the WRF model to produce storms with longer track lengths than radar storms (section 4.1.3) is likely due to the greater speed of the model storms compared to the radar storms. There seems to be no influence from storm duration on the results for track length.

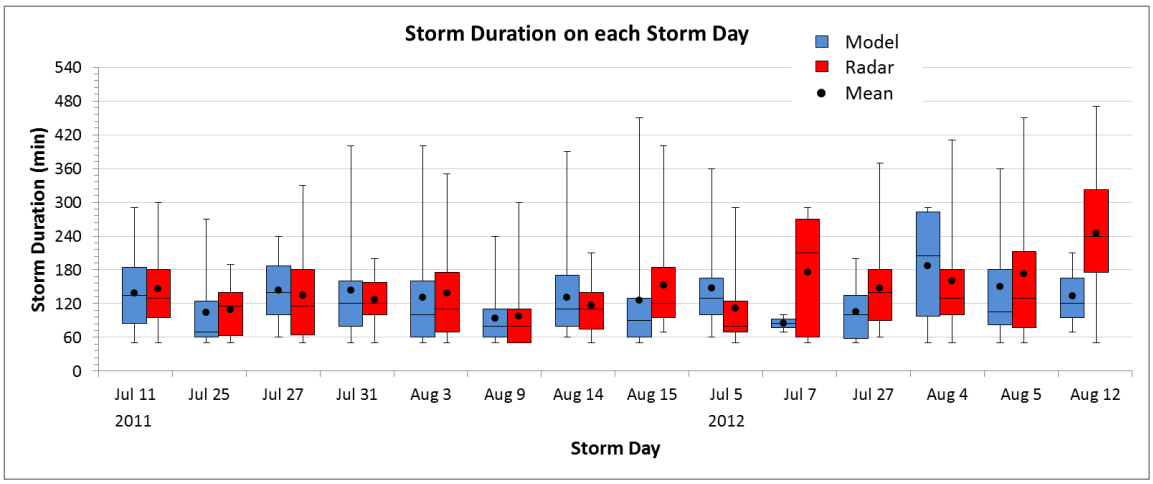

Figure 4-11. Duration (min) of the model and radar storms on each storm day. Box plots show median values (horizontal line), mean values (dot), 50th percentile values (box outline), and minimum and maximum values (whiskers).

After determining the time at which each model and radar storm achieved its maximum dBZ value after reaching the 35 dBZ track threshold, scatter plots were

produced of this time versus the storm duration. Figure 4-12 is a summary scatter plot of this comparison for every storm cell in this study. Of the 14 cases in this study, the time that the maximum dBZ value was reached after track initiation increases with track duration for the model and radar storms in 13 cases (93%) and 14 cases (100%), respectively. In the one model case that disagrees, the result is skewed by one cell that reached its maximum intensity very early (20 minutes after reaching the 35 dBZ track threshold) and lasted for a long time (360 minutes). Therefore, the longer the track duration, the more time it usually takes for a storm to reach its maximum dBZ value.

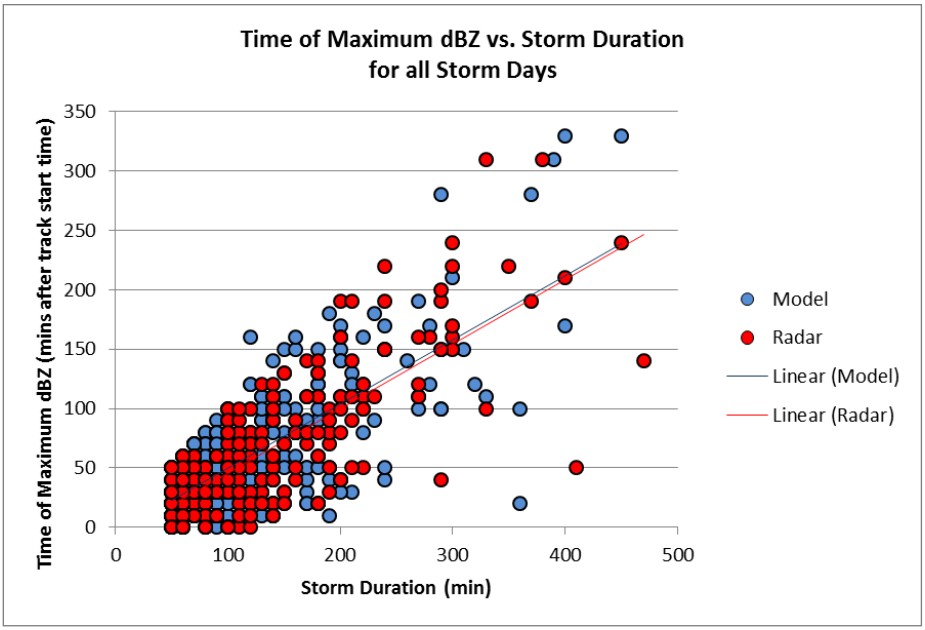

Figure 4-12. Relationship between the time of maximum dBZ (minutes after track start time) and storm duration (min) for the model and radar storms on all storm days.

Similar to the results for track length, we find that the model and radar storm duration decreases with increasing track start time in 10/14 cases (71%) and 13/14 cases (93%), respectively. Therefore, storm duration tends to decrease as storms initiate later in the day. Figures 4-13 and 4-14 show two storm days, 15 August 2011 and 5 August 2012, that exhibit this relationship for both the model and radar storms.

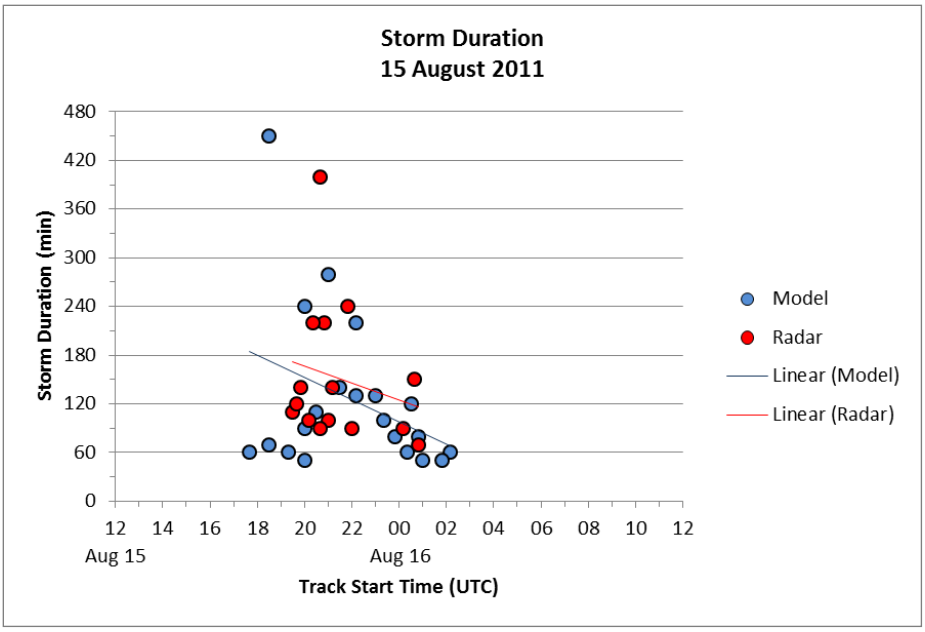

Figure 4-13. Duration (min) of the model and radar storms on 15 August 2011.

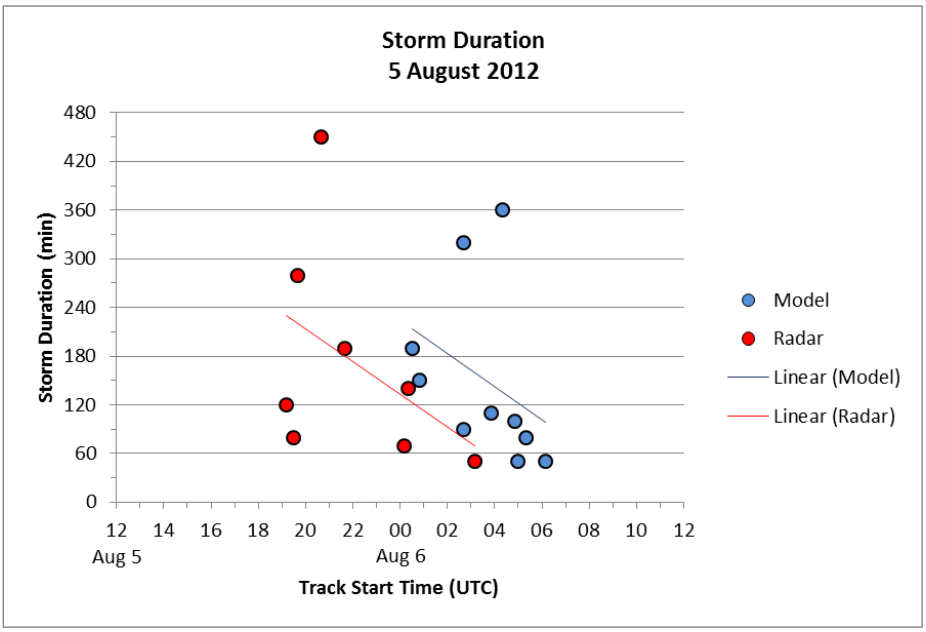

Figure 4-14. Duration (min) of the model and radar storms on 5 August 2012.

4.1.5 Intensity

All cases in this study have the minimum, maximum, mean, and median of maximum dBZ less for the model storms than for the radar storms (Figure 4-15). The model also produced storms with a smaller spread of maximum intensity compared to the radar storms, and the spread of track maximum dBZ between the lowest and highest value is less for the model than for the radar in 14/14 cases (100%), while the interquartile range is less for the model than for the radar in 12/14 cases (86%) (Figure 4-15). Therefore, the WRF model produces storms that are less intense in terms of maximum dBZ than radar-observed storms.

It was noticed quickly during track generation for this study that the WRF model produced less intense storms than those on radar. This influenced the selection of the 35 dBZ threshold that was used to select qualifying storm tracks. Originally we planned to use a threshold value of 45 dBZ because this value is the higher of the two user-defined intensity thresholds suggested for use within the TITAN storm cell identification algorithm, and is generally considered to represent severe storms with intense precipitation that may contain hail (Han et al. 2009); however, it was soon discovered that using this value would have eliminated too many model storms from the analysis. Therefore, the lower value of 35 dBZ was chosen. The fact that a model with 4 km resolution tends to produce cells that are larger in size than usually occurs in reality may influence cell intensity. It is possible that using a finer model grid resolution would allow the model to produce smaller storm cells having higher intensity.

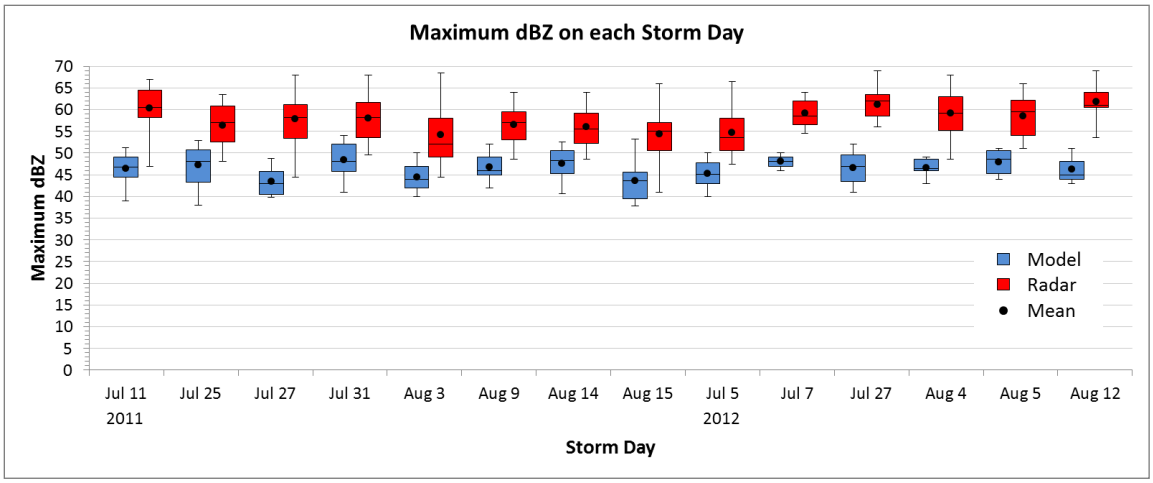

Figure 4-15. Maximum dBZ of the model and radar storms on each storm day. Box plots show median values (horizontal line), mean values (dot), 50th percentile values (box outline), and minimum and maximum values (whiskers).

From Figure 4-16 we see that the average maximum dBZ value of all model storms on a storm day tends to increase with the average maximum dBZ value of all radar storms; however, it does not increase as quickly. This means that the model does tend to produce stronger storms on days where the radar storms are stronger, but it does not match the magnitude of the intensity increase. It is likely that the discrepancy can be accounted for by the presence of hail in intense thunderstorms. When a storm contains hail this often acts to increase the dBZ value of the cell on radar since large pieces of wet ice are highly reflective. The WRF model attempts to account for hail production during convection by using a microphysics scheme. The Lin scheme (Lin et al. 1983) is used in this thesis, which includes five hydrometeor types: cloud water, cloud ice, rain, snow, and hail. It is possible that the scheme does not produce enough hail to match its prevalence within Alberta storms, or the simulated radar reflectivity field may not adequately represent the contribution of wet hail to the dBZ values. This is a suggested topic for further research.

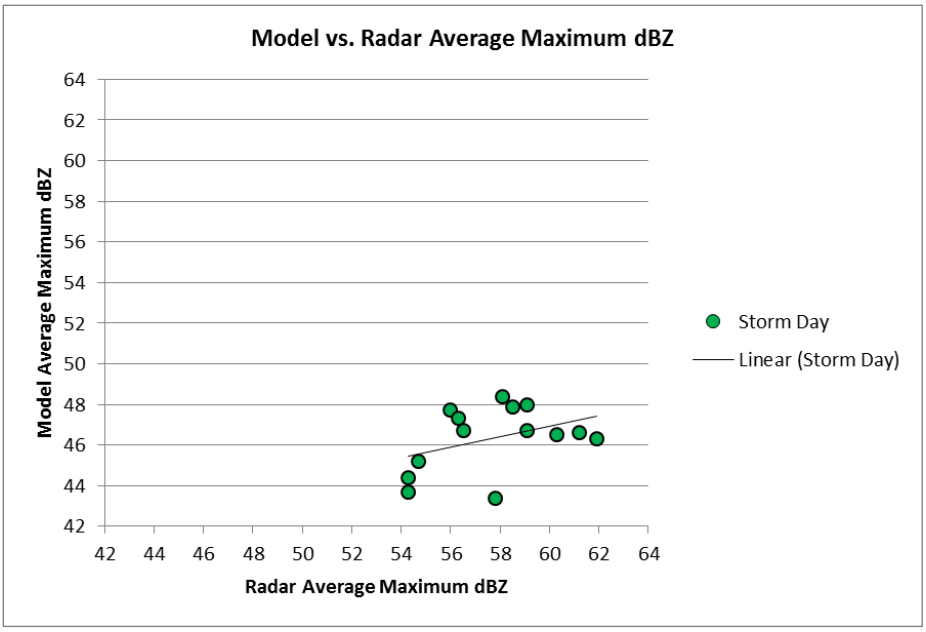

Figure 4-16. Relationship between the average of the maximum dBZ values reached by the model and radar storms on each storm day.

To explore any potential relationship between a storm's maximum dBZ and its start time, we graphed these values for all storm days in this study. We find that the maximum dBZ values of the model and radar storms decrease with increasing track start time in 11/14 cases (79%) and 12/14 cases (86%), respectively. Therefore, storm intensity (maximum dBZ) tends to decrease as storms initiate later in the day. This result is similar to the results for track length and duration in sections 4.1.3 and 4.1.4, respectively. Figures 4-17 and 4-18 show two storm days, 11 July 2011 and 4 August 2012, that exhibit this relationship for both the model and radar storms, as well as the tendency for model storms to have lower dBZ values than radar-observed storms.

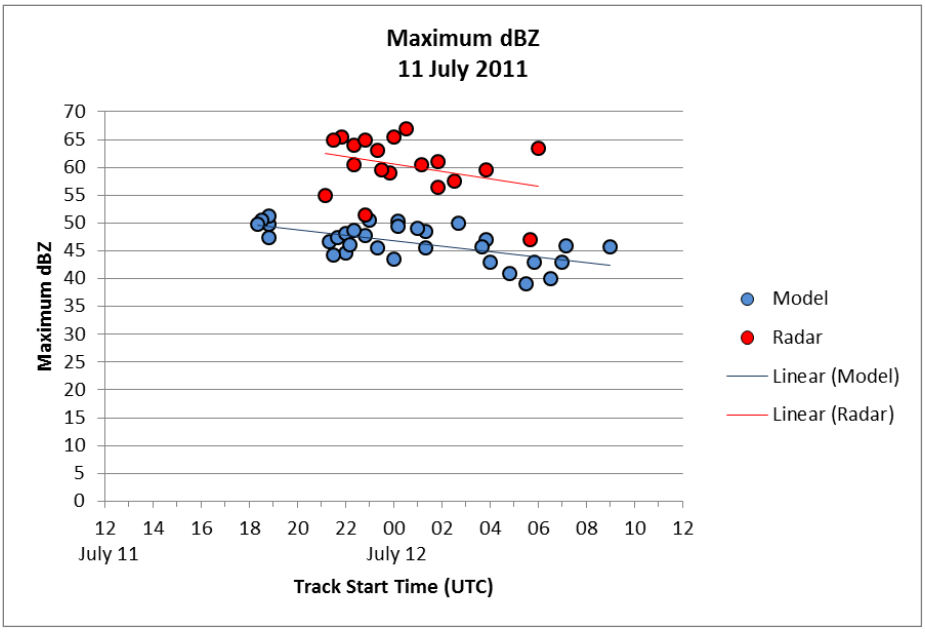

Figure 4-17. Maximum dBZ values reached by the model and radar storms on 11 July 2011.

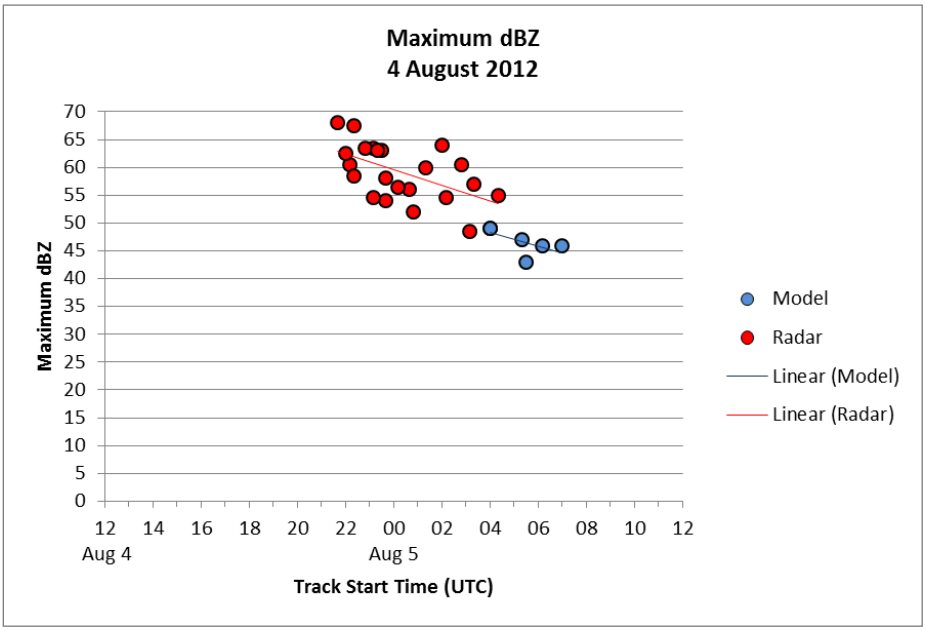

Figure 4-18. Maximum dBZ values reached by the model and radar storms on 4 August 2012.

A similar relationship to that above is found between track start time and the time during the storm day that the maximum dBZ value was reached by each storm cell.

The time of maximum dBZ for both the model and radar storms decreases with increasing track start time in 13/14 cases (93%) and 12/14 cases (86%), respectively. Therefore, the time it takes for a storm to reach its maximum intensity tends to decrease as it initiates later in the day. Figures 4-19 and 4-20 show this relationship for the same two storm days as in Figures 4-17 and 4-18, 11 July 2011 and 4 August 2012. These two days exhibit this relationship for both the model and radar storms.

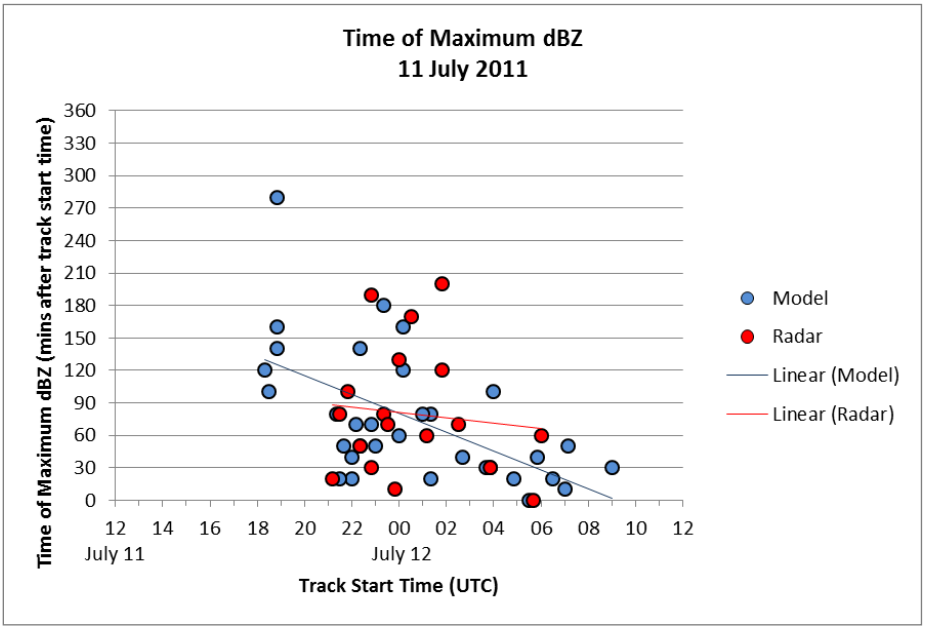

Figure 4-19. Time (in minutes after the track start time) that the maximum dBZ value was reached by each model and radar storm on 11 July 2011.

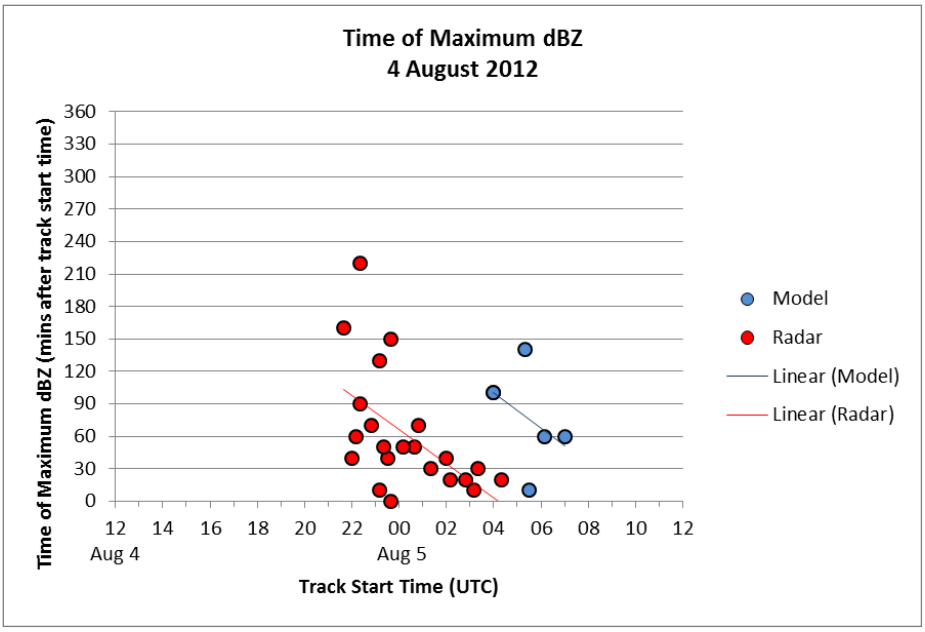

Figure 4-20. Time (in minutes after the track start time) that the maximum dBZ value was reached by each model and radar storm on 4 August 2012.

Additional analysis was done to look for relationships between track intensity (maximum dBZ) and storm speed, duration, and direction, with the expectation that storms with slower speeds, longer duration, and more clockwise track directions would have higher intensities (Bunkers et al. 2000, Mohee and Miller 2010). As mentioned in section 4.1.2, we find that a relationship may exist between storm intensity and direction such that storms with higher maximum dBZ values tend to have more clockwise tracks, or are possibly more right-moving. No relationship is found between storm intensity and speed or duration for either the model or radar-observed storms.

4.2 Storm initiation

This section presents the model results for storm start time and location. Though storm initiation is not the main focus of this thesis, it is important to mention how well the WRF model handles this component of the storm tracks since the selected tracks were dependent on storm initiation time and location during the track selection

process. To be clear, storm initiation in this thesis refers to the time when a storm first reaches the 35 dBZ intensity threshold. This is the beginning of a storm's track.

4.2.1 Time

Of the 14 storm cases in this study, 8 (57%) have the model initiating the first storm of the day, and 10 (71%) have the model initiating the last storm of the day (Figure 4-21). Of the 8 cases where the model initiates the first storm, 6 (75%) also have the model initiating the last storm of the day, after the last storm to initiate on radar. Thus the WRF model tends to initiate storms earlier and continue to initiate storms later than seen on radar. Additionally, 9/14 cases (64%) have the time between the first and last initiated storms greater for the model than for the radar, and 9/14 cases (64%) have the interquartile range greater for the model than for the radar (Figure 4-21). Therefore, the model produces storms with a larger spread of storm start times than radar-observed storms.

Figure 4-21 also shows that the median and mean of track start time occurs later for the model than for the radar in 11/14 cases (79%), and the beginning of the 4th quartile also occurs later for the model than for the radar in 11/14 cases (79%). Therefore, the model is skewed towards later start times for storms compared to radar-observed storms.

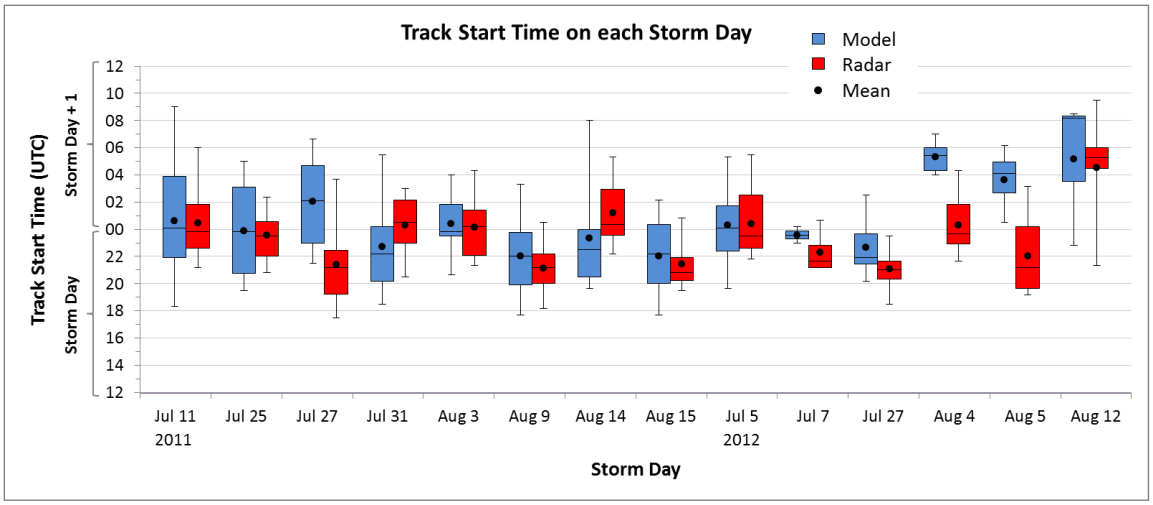

Figure 4-21. Start time (UTC) of the model and radar tracks on each storm day. Box plots show median values (horizontal line), mean values (dot), 50th percentile values (box outline), and minimum and maximum values (whiskers).

4.2.2 Location

We find that the WRF model initiates some storms farther south than those seen on radar in 9/14 cases (64%) and initiates some storms farther north in 8/14 cases (57%) in this study (Figure 4-22). Therefore, storms produced by the WRF model have a larger north-south area of initialization compared to radar-observed storms; however, the mean and the median of start latitude are greater for the model than for the radar in 9/14 cases (64%) which suggests that the model is also skewed towards more northerly start locations.

Despite the greater north-south span of initialization of the model, it is found that the spread of start latitudes for the model storms does not seem to be more than that of the radar storms. From Figure 4-22 we see that the latitudinal distance between the first and last model storm is greater than that of the radar storms in only 6/14 cases (43%), and the model interquartile range for start latitude is greater than that of the radar in only 5/14 cases (36%). Additionally, when analyzing Figure 4-22 qualitatively, the magnitude and spread of model storm start latitudes seem to be similar to those of the radar in almost all storm cases.

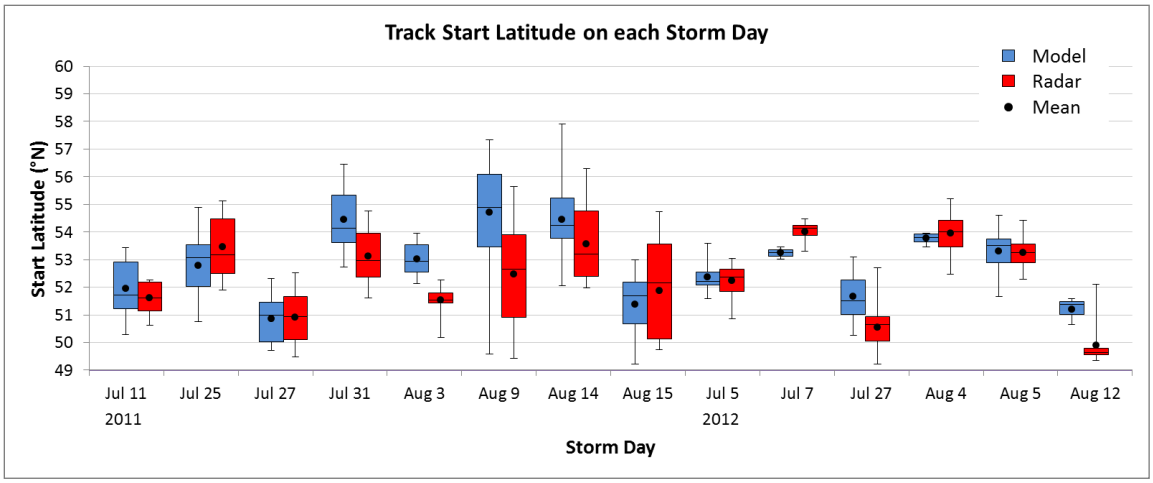

Figure 4-22. Start latitude (°N) of the model and radar tracks on each storm day. Box plots show median values (horizontal line), mean values (dot), 50th percentile values (box outline), and minimum and maximum values (whiskers).

Similar to latitude, we find that the WRF model initiates storms in a wider east-west area compared to radar-observed storms. From Figure 4-23 we see that the model initiates some storms farther west than those seen on radar in 9/14 cases (64%) and initiates some storms farther east in 9/14 cases (64%). We also see that the longitudinal distance between the first and last model storm is greater than that of the radar storms in 10/14 cases (71%), and the model interquartile range for start longitude is greater than that of the radar in 13/14 cases (93%). Therefore, the model has a larger spread of start longitude than radar-observed storms, which is unlike the corresponding result for latitude.

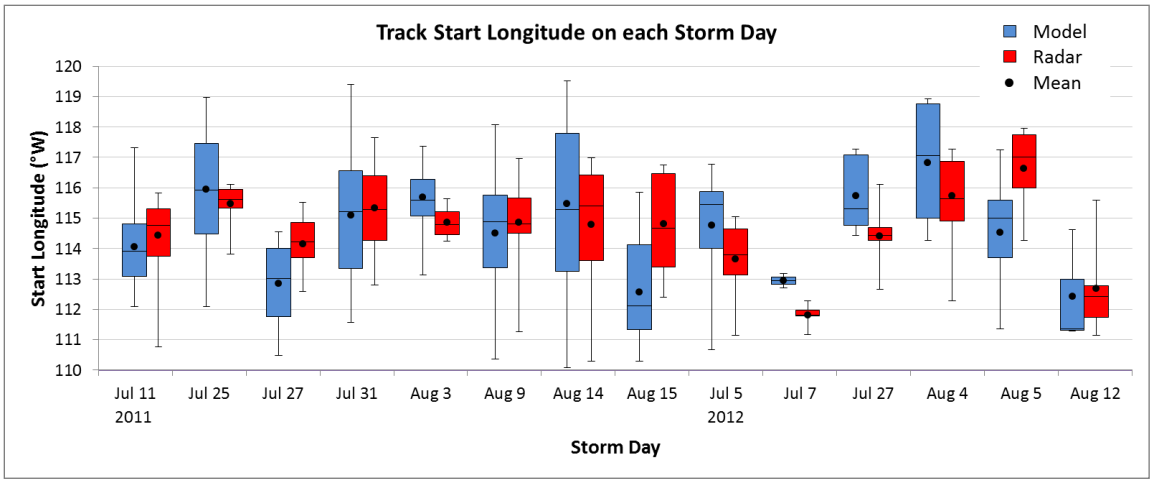

Figure 4-23. Start longitude (°W) of the model and radar tracks on each storm day. Box plots show median values (horizontal line), mean values (dot), 50th percentile values (box outline), and minimum and maximum values (whiskers).

Interesting trends were found between track start latitude, longitude, and time. Both the model and radar storms initiate farther south with start time in 9/14 cases (64%), while they initiate farther east with start time in 11/14 cases (79%) and 13/14 cases (93%), respectively. This suggests that storms in Alberta initiate farther south, as well as farther east, with time during a storm day. These trends may be attributable to the changing dynamics through a storm day such as changes in wind shear and its interaction with heat and moisture sources, and may follow a common pattern in Alberta that often results in northwest to southeast storm formation; however, more investigation into Alberta thunderstorm climatology needs to be done before reaching a formal explanation. Figures 4-24, 4-25, 4-26, and 4-27 show two storm days, 31 July 2011 and 3 August 2011, that exhibit these trends, along with the finding that the model is skewed towards more northerly start locations compared to radar-observed storms.

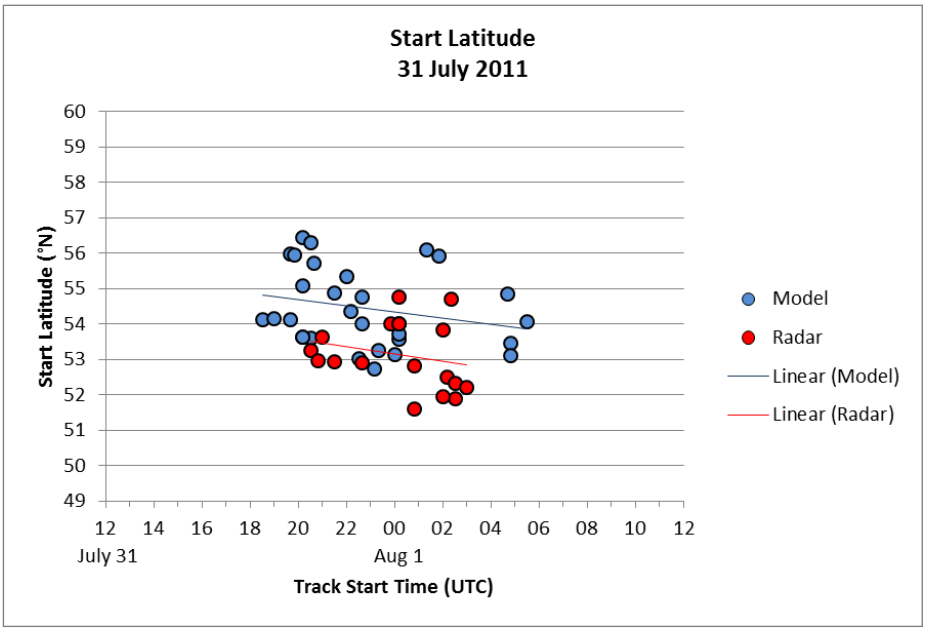

Figure 4-24. Start latitude (°N) of the model and radar tracks on 31 July 2011.

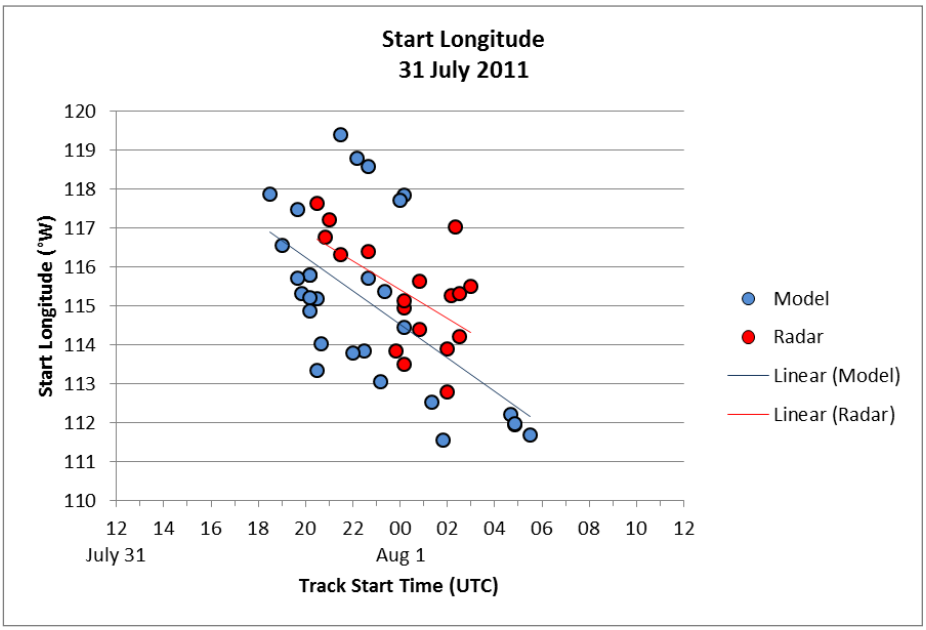

Figure 4-25. Start longitude (°W) of the model and radar tracks on 31 July 2011.

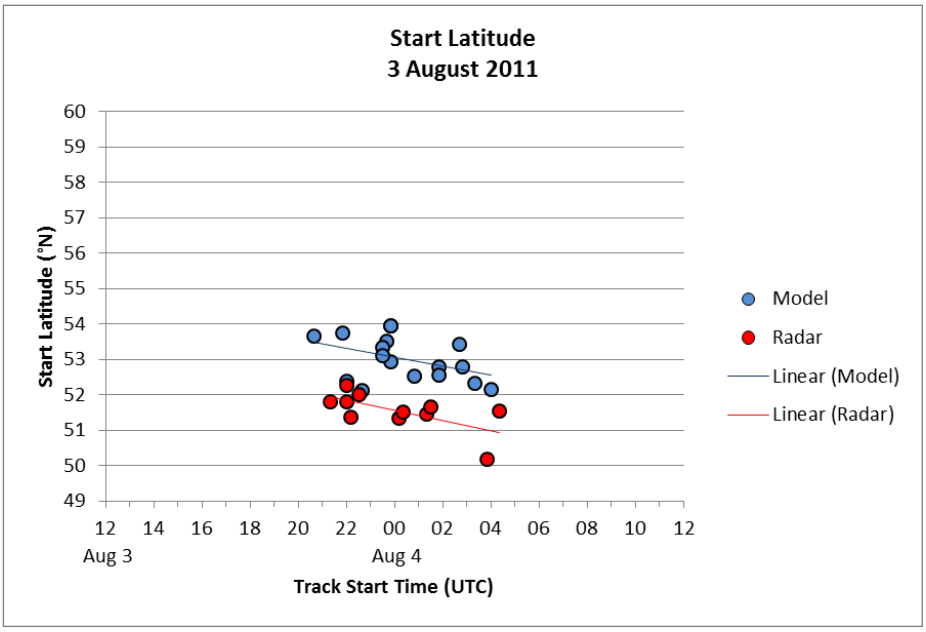

Figure 4-26. Start latitude (°N) of the model and radar tracks on 3 August 2011.

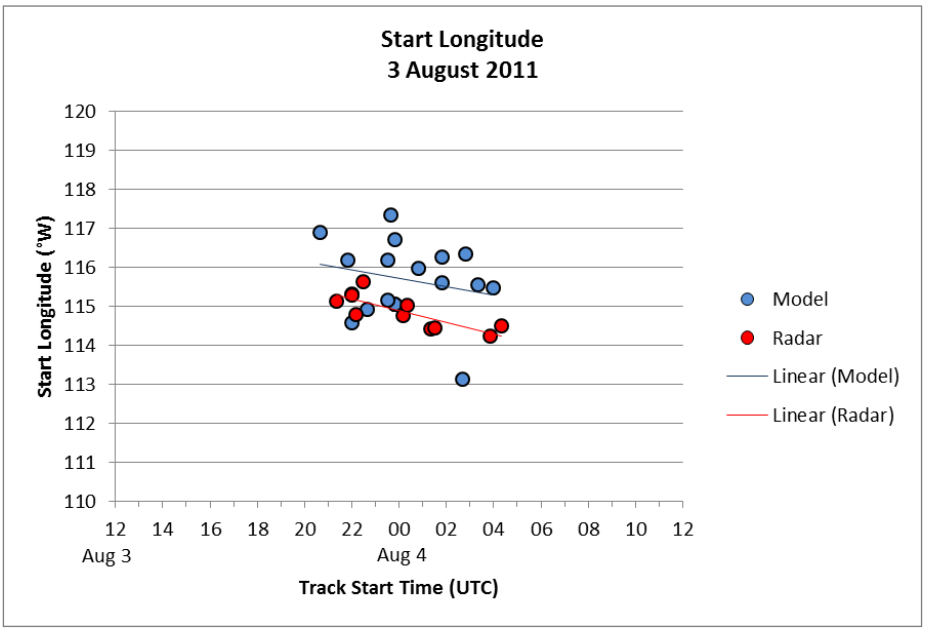

Figure 4-27. Start longitude (°W) of the model and radar tracks on 3 August 2011.

4.3 Summary of track comparison

This chapter presents the results of our comparison between the simulated storm tracks produced by the WRF model and the storm tracks observed on radar. We found that the WRF model produces storms that move faster, travel farther, and have more counter clockwise tracks than radar-observed storms. WRF storms are also less intense in terms of dBZ value, and they have shorter durations, though this is marginal. WRF storm intensity was found to increase with radar storm intensity, though not as quickly. We also found that WRF storm initiation time and location are more diverse, but are skewed towards later start times and more northerly start locations.

We found that the characteristics of storms tend to change as they develop later in the storm day. Storms that develop later in the day have shorter track lengths and shorter durations, and are less intense in terms of dBZ value. These storms also tend to be faster, though the WRF model did not replicate this trend. Also, the time it takes for a storm to reach its maximum intensity decreases as it initiates later in the day, and storm initiation location moves farther south and east.

WRF model storms and radar-observed storms having more clockwise tracks, or are possibly more right-moving, are found to last longer, travel farther, and reach higher intensities. This supports previous research on the characteristics of right-moving severe thunderstorms and supercells (Bunkers et al. 2000). These storms also tend to have slower speeds, though this did not hold for the WRF model storms in this study. An investigation into the accuracy of two storm motion forecast methods will be presented in chapter 5, along with a comparison between these methods and the WRF model storm tracks.

Chapter 5

Comparison between Model Sounding Derived Storm Motion and Observed Tracks

Storm motion is often predicted using the observed or forecast environmental winds. These winds are usually obtained from a sounding and presented using a hodograph. Though this technique cannot account for other factors that affect severe storm motion such as the surface fields of roughness, temperature, and humidity, it is relatively easy to employ on an observed or model sounding and there is no need to rely on the results of a high-resolution model and its explicit simulation of storms. This gives it the advantage of increased speed and flexibility since it can be used to determine forecast storm motion quickly in any area a forecaster deems favorable for storm formation.

Two common methods used for calculating severe storm motion are the Traditional (30R75) Method, which estimates storm motion to be 30° to the right and 75% of the magnitude of the mean wind in the lowest 6 km of the atmosphere (Maddox 1976), and Bunkers Method, which is Galilean invariant and therefore does not depend on the orientation of ground-relative winds (Bunkers et al. 2000).

This section presents the two methods, as well as the results of our investigation into how well these methods perform when used on WRF model forecast soundings. Forecast storm speed and direction is calculated using the Traditional Method and Bunkers Method on both the model and actual soundings at 0000 UTC from the Stony Plain, Alberta (WSE) sounding site, and this data is compared to the mean speed and direction of the simulated and observed storms for each storm day. The time of 0000 UTC is chosen as the time of comparison because it is representative of the day's storm environment as well as being the time that the actual sounding is taken each day at Stony Plain.

5.1 Traditional Method

The Traditional (30R75) Method of calculating storm speed and direction was developed by Maddox in 1976 and suggests that a severe thunderstorm or supercell in the Northern Hemisphere will move 30° to the right of the mean wind direction with a speed that is 75% of the magnitude of the mean wind. The mean wind is calculated through the lowest 6 km of the atmosphere and is referred to as the 0-6 km mean wind (Appendix B). The 0-6 km layer is used to calculate the mean wind because storm motion is most sensitive to the wind in these lower levels of the atmosphere (Wilhelmson and Klemp 1978). Storms often move slower than the mean wind speed due to the transfer of momentum deficit from lower to higher levels within updrafts. Strong storms will veer due to internal dynamics which depend largely on the vertical wind shear (Zeitler and Bunkers 2005, Bunkers et al. 2000).

It is known that the Traditional Method is an imperfect predictor of storm motion. It is an empirical relationship derived from severe storm motion in the eastern United States and it has been found to inaccurately forecast storm motion over Alberta (Krauss and Sinkevich 2007B). It also cannot predict the motion of left-moving storms (Krauss and Sinkevich 2007B); however, it continues to be used within forecast operations because it is easy to employ on an atmospheric sounding and it gives a rough estimate of right-moving storm motion, which is the most commonly observed storm motion over Alberta.

5.1.1 Speed

Figure 5-1 gives the difference between the mean speed of the model and radar storms for each storm case in this study, as well as the difference between the mean speed of the radar-observed storms and the forecast storm speed from the 0000 UTC model and actual soundings using the Traditional Method. From this figure we see that the model storms are generally faster than the radar storms, which is consistent with

the findings in section 4.1.1. We also see that the forecast storm speeds calculated using the WRF model soundings underestimate both the model and radar storm speeds for all 14 cases. When we compare the forecast speeds from the model soundings to those from the actual soundings at Stony Plain (WSE), we find that the Traditional Method also gives storm speeds that are less for the model soundings than for the actual soundings in all cases. This is unexpected because the WRF model has a positive storm speed bias as presented in section 4.1.1. Therefore, one would expect that using the Traditional Method on the model sounding would also give an overestimation of the forecast storm speed relative to that from the actual sounding, but this is not the case. The Traditional Method actually gives an even greater underestimation of storm speed when used on the model soundings than when used on the actual soundings.

Additionally, 13/14 cases (93%) have the 0000 UTC actual sounding forecast speed less than both the model and radar storm speeds. Therefore, we can conclude that the Traditional Method underestimates storm speed for both the model and actual soundings, and gives an even greater underestimation of speed when used on the WRF model sounding data from 0000 UTC.

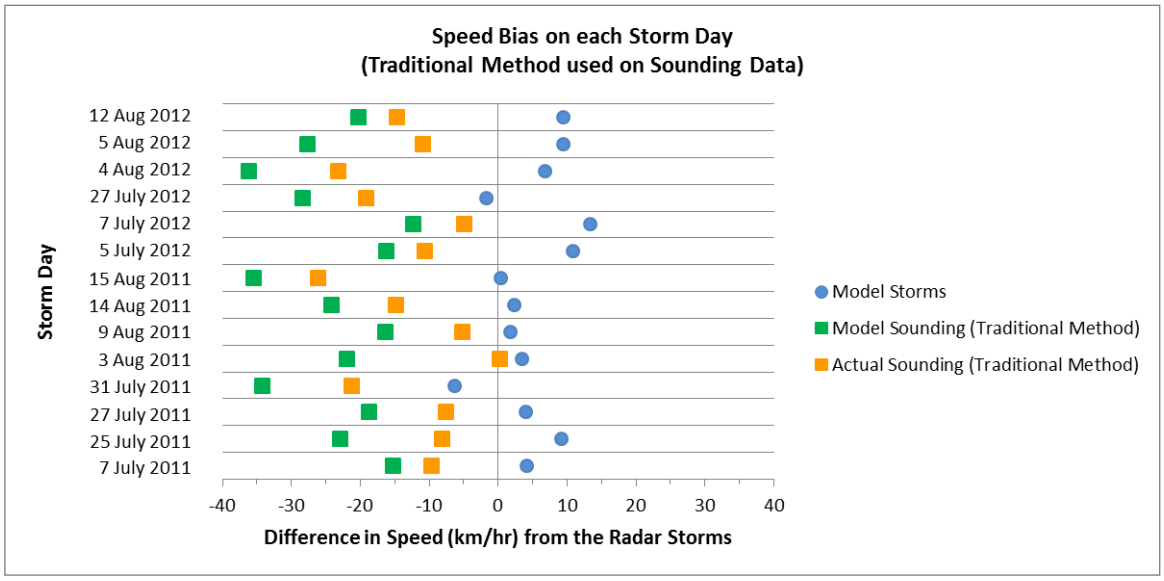

Figure 5-1. Difference between the mean speed (km/hr) of the model storms and the mean speed of the radar storms for each storm day, as well as the speed bias of the Traditional Method when used on the model and actual soundings.

5.1.2 Direction

Figure 5-2 shows the difference between the mean direction of the model and radar tracks for each storm case in this study, as well as the difference between the mean track direction of the radar-observed storms and the forecast storm direction from the 0000 UTC model and actual soundings using the Traditional Method. A positive difference in direction for an element in the figure means that the forecast storm direction of that element is more clockwise than the mean direction of the radar tracks. A negative difference in direction means that the forecast storm direction is more counter clockwise than the mean direction of the radar tracks. From this figure we see that the Traditional Method used on the WRF model soundings tends to give forecast storm direction values that are more clockwise, or possibly more right-moving, than both the model and actual storm tracks. This is true for 13/14 storm cases (93%) in this study. The Traditional Method used on the actual soundings also tends to give storm direction values that are more clockwise than both the model and actual storm tracks.

This is true for 12/14 storm cases (86%) in this study. Therefore, the Traditional Method can be said to overestimate storm direction.

When comparing the forecast storm directions using the Traditional Method for both the model and actual soundings, we find that only 7/14 cases (50%) have the forecast direction from the model sounding greater, or more clockwise, than from the actual sounding (Figure 5-2). Therefore, it is unclear whether there is a relationship between the forecast storm directions from these two sounding sources when using the Traditional Method. This is interesting because it was determined in section 4.1.2 that the WRF model tends to produce storms with track directions that are more counter clockwise, or possibly less right-moving, than storms on radar, and so it was expected that this relationship would also hold between the model and actual sounding forecast directions given by the Traditional Method; however, this is not the case.

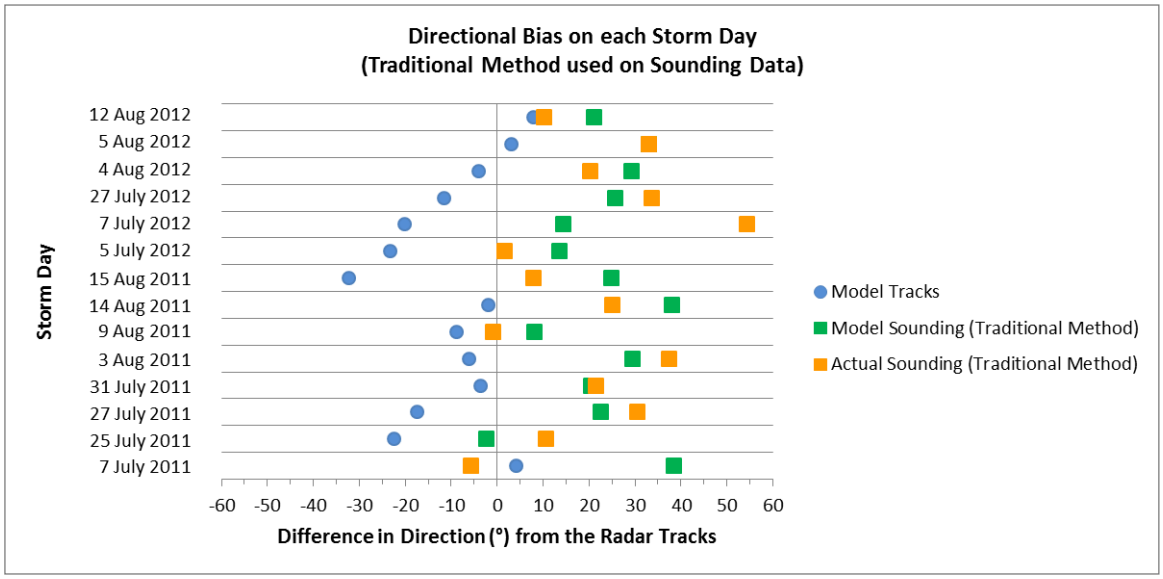

Figure 5-2. Difference between the mean direction (°) of the model tracks and the mean direction of the radar tracks for each storm day, as well as the directional bias of the Traditional Method when used on the model and actual soundings.

5.2 Bunkers Method

Bunkers et al. (2000) proposed a new method for predicting the speed and direction of supercells using a hodograph. It suggests that there are two main components of supercell motion: advection by the 0-6 km mean wind, and propagation away from the mean wind towards the left or the right of the vertical wind shear due to internal storm dynamics. The calculation of forecast storm motion using Bunkers Method on a hodograph is given in Appendix C.

The motivation behind the development of this new method was taken from studies on storm motion within different storm environments. It was found that previous methods of predicting storm motion such as the Traditional Method tend to work best when used in a "typical" storm environment, which is one where the vertical wind shear is strong and oriented in the upper right quadrant of the hodograph. Bunkers et al. (2000) sought to develop a method that would predict both right- and left-moving supercells in all storm environments. Bunkers Method is Galilean invariant, meaning that it does not depend on the orientation of the ground-relative winds, and it has been shown to better predict the motion of right- and left-moving supercells compared to previous methods, especially in non-typical storm environments (Bunkers et al. 2000). Although Bunkers Method gives predictions for both right- and left-moving storms, only the speed and direction for right-moving storms will be considered in the following analysis. Right-moving storm motion is the most commonly observed motion for severe storms over Alberta.

5.2.1 Speed

Of the 14 cases in this study, 12 (86%) have the Bunkers' forecast storm speed for the WRF model sounding less than the mean of the model storm speeds (Figure 5-3). Bunkers Method also tends to underestimate the radar storm speeds, with 9/14 cases in this study (64%) having the Bunkers' forecast storm speed using the model sounding less

than the mean of the radar storm speeds (Figure 5-3). Therefore, it can be said that Bunkers Method tends to underestimate storm speed when used on the 0000 UTC model soundings.

When we compare the forecast speeds based on the model soundings to those based on the actual soundings at Stony Plain (WSE) we find that Bunkers Method also gives speeds that are less for the model soundings than for the actual soundings in 12/14 cases (86%) (Figure 5-3). This is similar to the results from the Traditional Method in section 5.1.1; however, in contrast to the Traditional Method, the actual sounding forecast speed is greater than the mean model storm speed in 7/14 cases (14%) and greater than the mean radar storm speed in 12/14 cases (86%). Therefore, Bunkers Method tends to overestimate storm speed when used on the actual soundings, but tends to underestimate storm speed when used on the model soundings.

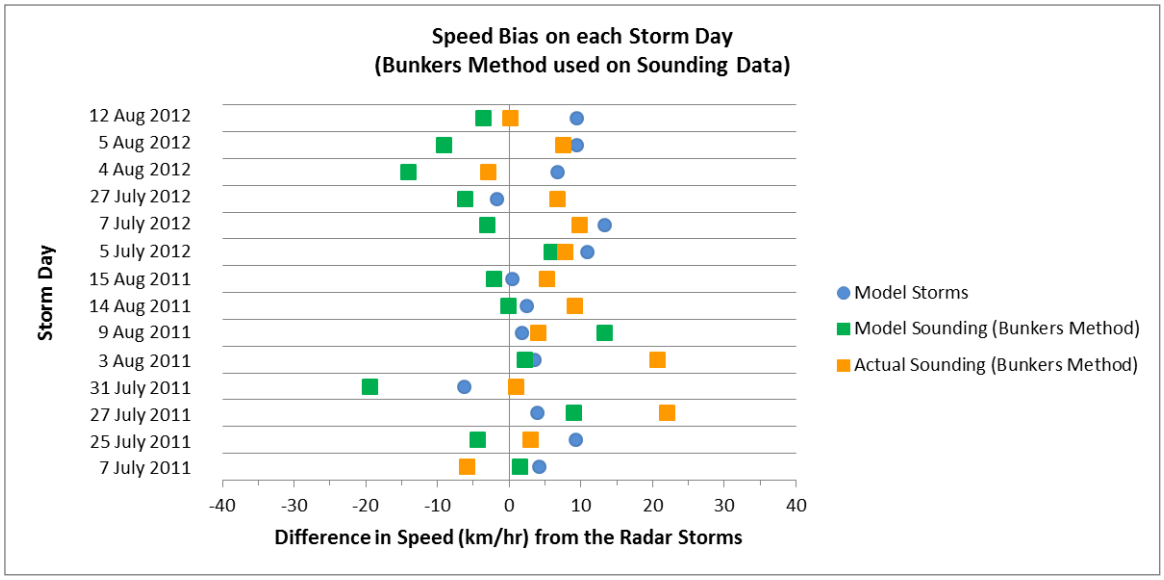

Figure 5-3. Difference between the mean speed (km/hr) of the model storms and the mean speed of the radar storms for each storm day, as well as the speed bias of Bunkers Method when used on the model and actual soundings.

5.2.2 Direction

Figure 5-4 shows the difference between the mean direction of the model and radar tracks for each storm case in this study, as well as the difference between the mean track direction of the radar-observed storms and the forecast storm direction from the 0000 UTC model and actual soundings using Bunkers Method. From this figure we find that Bunkers Method used on the WRF model soundings tends to give forecast storm direction values that are more clockwise, or possibly more right-moving, than both the model and actual storm tracks. This is true for 13/14 storm cases (93%) in this study. In one of these cases, 7 July 2012, the model forecast storm direction using Bunkers Method is actually 115° more clockwise than the direction of the radar tracks. The forecast direction in this case is 3° while the mean direction of the radar tracks is a more realistic value of 248°. Bunkers Method used on the actual soundings also tends to give storm direction values that are more clockwise, or possibly more right-moving, than both the model and actual storm directions. This is true for 13/14 storm cases (86%) in this study. In one of these cases, 7 July 2011, the forecast storm direction using Bunkers Method on the actual sounding is 185° more clockwise than the direction of the radar tracks. This is completely opposite in direction. The forecast direction in this case is 10° while the mean direction of the radar tracks is 195°. From these results, Bunkers Method can be said to overestimate storm direction.

When we compare the forecast storm directions from Bunkers Method for both the model and actual soundings, we find that 11/14 cases (79%) have the model sounding forecast direction more clockwise than the actual sounding forecast direction (Figure 5-4). Therefore, it can be said that Bunkers Method tends to overestimate storm direction, with an even greater degree of overestimation when used on the WRF model soundings.

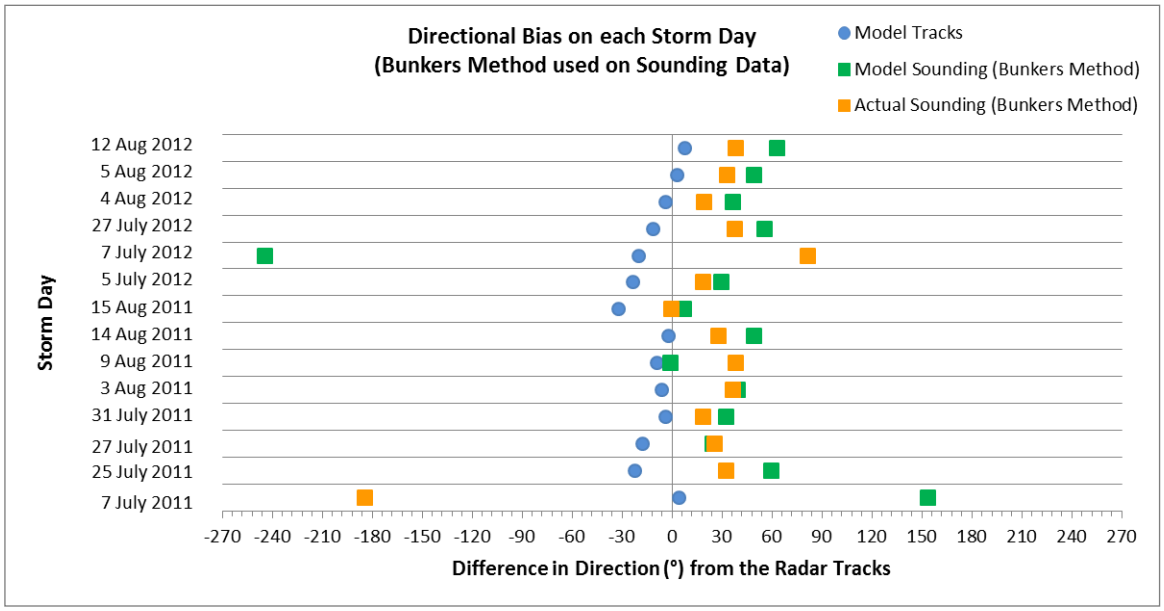

Figure 5-4. Difference between the mean direction (°) of the model tracks and the mean direction of the radar tracks for each storm day, as well as the directional bias of Bunkers Method when used on the model and actual soundings.

5.3 Comparison between Traditional and Bunkers Methods

In order to provide a qualitative assessment of the comparative accuracies of the Traditional Method and Bunkers Method, the conclusions in this section are based on a qualitative inspection of the data presented in sections 5.1 and 5.2. We find that Bunkers Method is generally more accurate for estimating storm speed; however, the results are less predictable than for the Traditional Method in that it is not known whether the speed is underestimated or overestimated in each forecast case, and by how much. The Traditional Method tends to greatly underestimate storm speed, but the amount by which it underestimates the speed tends to be more consistent.

We find that the Traditional Method is generally more accurate and consistent overall than Bunkers Method for estimating storm direction. Though both methods tend to overestimate the storm direction, or give more clockwise storm directions compared to radar-observed storms, the Traditional Method is more consistent in its overestimation and more closely matches the values of the model and radar storm

directions. Also, Bunkers Method gives some cases of estimated northeasterly storm directions that do not occur in reality. The Traditional Method does not produce these results.

Chapter 6

Conclusion

6.1 Conclusion and discussion of thunderstorm track comparison

This thesis examines the accuracy of the WRF model for simulating the motion of severe thunderstorms over Alberta. There has been a lack of research on the convective forecast skill of cloud-scale models for the motion of thunderstorms despite the increasing prevalence of high-resolution model data and the continued need for accurate storm motion forecasts. To address this topic, the WRF model was used to simulate thunderstorm development over Alberta for several days in 2011 and 2012 using a resolution of 4 km and without the use of a cumulus parameterization scheme. Storm tracks were then created from the model output and were compared to the tracks of radar-observed storms using CAPPI 1.5 km radar data. An emphasis on the motion and intensity of the storms was given during track comparison.

The severe storm tracks produced by the WRF model in this study generally agreed well with the radar-derived tracks on the selected storm days; however, some key differences were found. The WRF model tends to produce storms that move faster than radar-observed storms. To narrow down a reason for this bias we must consider the results from section 5.1.1. In this section we compared the mean speeds of the model and radar storms to the forecast storm speeds given by the Traditional Method when used on the WRF model soundings and actual soundings from Stony Plain, Alberta. We found that the Traditional Method underestimates the speed of the model and radar storms when used on the actual soundings, and gives an even greater underestimation of storm speed when used on the model soundings. This suggests that the main cause for the WRF model's positive storm speed bias does not originate with the model winds in the 0-6 km layer, otherwise the Traditional Method would have given forecast storm speeds that were faster for the model soundings than for the

actual soundings, to match the relationship between the model and radar storm speeds. The cause of the WRF model storm speed bias is a suggested topic for further research.

We found that the WRF model storms tend to move in a more counter clockwise direction compared to radar-observed storms. We also found that track length, storm duration, and storm reflectivity (dBZ) tend to increase with track direction for both the model and radar storms, suggesting that storms with more clockwise tracks tend to last longer, travel farther, and reach higher intensities. This agrees with previous research on severe thunderstorms and supercells (Bunkers et al. 2000, Zeitler and Bunkers 2005). These findings suggest that the 4 km resolution WRF model is able, to some degree, to resolve and simulate these right-moving storms and to replicate their motion; however, it is known that severe right-moving storms often move slower than non-severe storms and this relationship was found to hold for the radar storm tracks in this study but was inconclusive for the WRF model tracks. Therefore, the model cannot completely and realistically simulate the internal dynamics and interactions between a storm and the environmental wind at 4 km resolution.

The WRF model tends to produce storms that have a longer track length than radar-observed storms. WRF model storms also tend to have a slightly shorter lifespan, though this is marginal. Storm track length and duration also tend to decrease with increasing track start time so that cells initiating later in the storm day tend to have a shorter duration and not travel as far as those initiating earlier. The implementation of a minimum threshold value for track duration likely influenced these results, particularly for storm cases with many tracks that are at or close to the threshold value. For example, the tendency for WRF model storms to have a shorter lifespan than storms on radar may become more pronounced if the duration threshold value was lowered to include more tracks with durations of less than 50 minutes.

The fact that WRF model storms tend to travel greater distances than storms on radar seems to be due to the fact that they also tend to have greater speeds, despite having slightly shorter lifespans. Track length and duration may decrease with track start time because the favorability of conditions for storm development and maintenance

decreases through the end of a storm day. Of course, this depends on the day's storm dynamics and storm mode. Supercell storms tend to last longer because of the separation of updraft and downdraft and their internal rotation, and elevated convective storms can have the proper dynamics to be strengthened rather than defeated by nocturnal surface and cloud top cooling through the night.

Our results show that the WRF model produces storms that are less intense, in terms of maximum dBZ, than storms on radar. This result may be due to a combination of factors. It is very possible that the CAPPI 1.5 km radar data is overestimating the rainfall rate within storms due to the presence of hail, which is common in convective storms on the Prairies. Also, the Lin microphysics scheme (Lin et al. 1983) used in this thesis may not produce enough hail to match its prevalence within Alberta storms, or the simulated radar reflectivity field may not adequately represent the contribution of wet hail to the dBZ values. The model also tends to produce cells that are much larger in size than reality when using a 4 km grid resolution, and this may influence model storm intensity. It is possible that using a finer grid resolution would allow the model to produce smaller storm cells having higher intensity. Also, the radar and model track intensity was measured at the CAPPI 1.5 km level or 750 mb. This is likely to have some effect on the results. Through their lifetimes storms tend to change where the highest reflectivity values are in the vertical, shifting from below the 750 mb level to above it as a storm matures, and back to below as a storm decays. This may cause an underestimation of a storm's intensity when only measuring at one level.

We found that maximum storm reflectivity tends to decrease with track start time so that storm intensity decreases as storms initiate later in the day. The time that it takes for a storm to reach its maximum intensity also decreases as it initiates later in the day. Similar to track length and duration, the decreased number of hours of favorable storm conditions at the end of a storm day may limit the maximum intensity that can be achieved by a developing cell. Storm cells may develop more rapidly later in the day, though, because of the buildup of potential energy that is then released "explosively." There also tends to be an abundance of triggers for storm formation later in the day,

with multiple converging gust fronts and high surface heat and humidity, and this can lead to rapid storm development, though the resulting storms are not as intense or long-lived.

Though storm initiation was not the focus of this thesis, the results for the timing and location of initiation of WRF model storms were presented as important components of a storm's track. It was found that the WRF model tends to initiate storms earlier and continue to initiate storms later than seen on radar, and that the model storms tend to be skewed towards later start times. Since the WRF model was run without the use of a cumulus parameterization scheme, it explicitly created storms when there was instability at a grid point, and this release was instantaneous. In reality, it is common for there to be an atmospheric cap on the instability, allowing energy to build up until its release when the cap is broken by processes such as surface heating and mid-level cooling ahead of an upper trough. Similarly, the model may continue to release energy and create storms later than seen on radar because of a delay in the development of the nocturnal inversion and the lower-level stabilization that this causes. Also, the size of a model storm within a 4 km resolution grid tends to be larger than the average radar-observed storm. Therefore, it may take longer for model storms to reach the 35 dBZ intensity threshold than radar-observed storms, and this may have caused the skew towards later start times for the model storms.

We found that the WRF model tends to produce storms in a wider area of initialization in both the north-south and east-west directions. This may be due to several factors. First, in this study the storm "start location" is really the geographic location at which a storm first reaches the threshold intensity value of 35 dBZ. Therefore, the speed and direction of a storm may influence its start location. For example, it was found that the WRF model produces storms that move faster than storms on radar. Therefore, if these storms initiate along the foothills and travel east, which is typical in Alberta, these storms may reach the 35 dBZ threshold farther east than radar-observed storms because of their faster speeds.

Our results may also be influenced by the restriction that storm cells must have initiated within Alberta and had their entire track within Canadian radar coverage. It could also be that the WRF model is less influenced by topography as a storm trigger, which may or may not be due to model grid resolution or the representation of topography within the model. In Alberta, the topography of the foothills often serves as the trigger for storms due to differential heating along the east-facing slopes and the creation of moisture gradients and destabilization in upslope flow (Smith and Yau 1993).

6.2 Conclusion and discussion of storm motion forecasts using Traditional and Bunkers Methods

This thesis examines how well the Traditional and Bunkers Methods of forecasting storm motion perform when used on WRF model forecast soundings. These methods are frequently used by forecasters to predict storm motion in advance of storm formation. For this study, these methods were employed on model and actual 0000 UTC soundings from Stony Plain, Alberta (WSE) on each selected storm day in the summer months of 2011 and 2012. The results were then compared to each other, as well as to the model and radar storm track data to assess the accuracy of the methods.

We found that both the Traditional Method and Bunkers Method tend to underestimate storm speed when used on the WRF model soundings. Both methods also tend to give slower storm speeds when used on the model soundings than when used on the actual soundings at 0000 UTC. This is an interesting result given the fact that the WRF model tends to produce storms that are faster than radar-observed storms, so it was expected that both methods would also give faster speeds when used on the model soundings; however, this was not the case.

Additionally, when compared to the model and radar track results, both forecast methods tend to underestimate the model and radar storm speeds when used on the WRF soundings. When used on the actual soundings, Bunkers Method tends to overestimate the model and radar storm speeds while the Traditional Method does not.

We found that both the Traditional Method and Bunkers Method tend to overestimate storm direction when used on the WRF model soundings, giving forecast storm directions that are more clockwise, and possibly more right-moving, than radar-observed storms. When used on the actual soundings, both methods also tend to overestimate storm direction, but at a slightly less magnitude for Bunkers Method. It would be interesting to examine whether there are any major differences in the vertical wind shear vectors from the model and actual soundings, as well as in the shape of the associated hodographs, and whether these contribute to the differences in storm motion forecasts produced by Bunkers Method when used on the two different sounding sources. This is a suggested topic for further research.

Our results may lead one to suggest that both the Traditional and Bunkers Methods do not perform well in Alberta, especially when the explicit simulation of storms by the WRF model tends to produce more accurate results; however, we should be cautious when coming to this conclusion. Both the Traditional and Bunkers Methods were developed to estimate the motion of severe storms and supercells using statistics from storms primarily observed in central and eastern regions of the United States. The majority of the storm cells in this study likely do not fall into the supercell category and do not reach heights or intensities as great as those found in regions farther south. Therefore, it makes sense that both of these methods would tend to underestimate the speed and overestimate the direction of storm cells given that severe storms and supercells tend to move slower and propagate farther to the right of the mean wind than other cells.

After comparing the results from the Traditional Method and Bunkers Method, it is found that Bunkers Method is generally more accurate for estimating storm speed in Alberta, but the results are less predictable than from the Traditional Method. The Traditional Method tends to greatly underestimate storm speed, but the amount by which it underestimates the speed tends to be more consistent. For estimating storm direction, the Traditional Method is generally more accurate and consistent, though both methods tend to overestimate the value.

6.3 Recommendations for further research

This section presents suggestions for further research on the topic of WRF model storm tracks. As mentioned previously in sections 6.1 and 4.1.5, respectively, it would be valuable to determine why the WRF model produces storms that move faster and are less intense than radar-observed storms. An investigation into storm intensity could include a comparison of WRF simulation results using different microphysics schemes to determine their effect, if any, on the simulated dBZ values. Also, as suggested in section 6.2, a comparison between the hodograph shape and vertical wind shear vectors from the model and actual soundings may help us understand why Bunkers Method produces different storm motion forecasts when used on the two different sounding sources.

During the storm day selection process there was no distinction made between storm days with different storm environments. The only restriction imposed on the storm day selection was to eliminate days with convection dominated by mesoscale features. If each case was examined and a decision made as to whether the storm environment was "typical" for Alberta or not and what the dominant storm mode was, then the days could be separated into categories based on these characteristics. This would allow for a more in-depth analysis of how the WRF model handles each of these scenarios. For example, is the WRF model more accurate for storm development in a "typical" Alberta storm environment? Is the WRF model more accurate on days with little potential for supercell development, or on very severe days with high environmental wind shear? Do the Traditional Method and Bunkers Method perform better on days with greater potential for supercells? Is Bunkers Method more accurate than the Traditional Method on days that are less "typical?" These are some of the questions that could be answered by dividing storm days into categories based on storm environment.

There were also multiple references to right-moving storms in this thesis and there was an implied correlation between right-moving storms and those storms with track directions that had a more clockwise component. This correlation was made

because each track direction was calculated as a straight line based on the mean direction of travel of each cell. No analysis of track curvature was made in this thesis. It may be insightful to determine the curvature of each model and radar storm track, whether to the right or to the left of the mean wind, and then examine how realistically the WRF model handles this important storm track characteristic.

Another characteristic that would be interesting to analyze is the width of the storm tracks, either based on the horizontal diameter of the 35 dBZ contour or by some other means. By analyzing the widths of the tracks, one could determine whether the growth and dissipation of the WRF model cells match the pattern found for radar-observed cells.

One last recommendation for further research is a comparison of storm tracks extracted from different radar products. This thesis gathered observed storm tracks from CAPPI 1.5 km radar data, but would the storm tracks gathered from other radar products such as maximum reflectivity within the column significantly change the observed track dataset? This would be a valuable determination, and would aid the design of future studies involving thunderstorm tracks.

References

Bunkers, M., Klimowski, B., Zeitler, J., Thompson, R., & Weisman, M. (2000). Predicting supercell motion using a new hodograph technique. *Weather and Forecasting 15*, 61-79.

Bunkers, M. (2002). Predicting supercell motion using hodograph techniques. *Weather Forecast Office Rapid City, South Dakota.* (Last updated 4 February, 2002). Retrieved 7 August, 2015, from www.crh.noaa.gov/Image/unr/soo/scm/SCmotion.ppt.

Burrows, W., King, P., Lewis, P., Kochtubajda, B., Snyder, B., & Turcotte, V. (2002). Lightning occurrence patterns over Canada and adjacent United States from lightning detection network observations. *Atmosphere-Ocean 40*(1), 59-80.

Cain, D. & Kirkwood, P. (2005). WSR-88D Radar FAQ's. *National Weather Service, National Oceanic and Atmospheric Administration* (Last updated 3 March, 2005). Retrieved 20 August, 2012, from http://www.srh.noaa.gov/radar/radinfo/radinfo.html.

Calgary Herald. (2014). The flood's tragic toll: Remembering the five lives lost. *Calgary Herald* (Last updated 12 June, 2014). Retrieved 27 May, 2015, from http://www.calgaryherald.com/news/alberta-floods-2013/flood+tragic+toll+Remembering+five+lives+lost/9937864/story.html.

Chen, F. & Dudhia, J. (2001). Coupling an advanced land surface-hydrology model with the Penn State-NCAR MM5 modeling system. Part 1: Model implementation and sensitivity. *Monthly Weather Review 129*, 569-585.

Cheng, D., Mercer, R., Barron, J., & Joe, P. (1996). Tracking fuzzy storm centres in Doppler radar images. *IEEE International Conference on Image Processing (ICIP1996)*, Lausanne, Switzerland, 16-19 September, 1996, Vol. 2, 959-962.

Corfidi, S. (2003). Cold pools and MCS propagation: Forecasting the motion of downwind developing MCSs. *Weather and Forecasting 18*, 997-1017.

Davies, J. & Johns, R. (1993). Some wind and instability parameters associated with strong and violent tornadoes. Part I: Wind shear and helicity. *The Tornado: Its Structure, Dynamics, Prediction, and Hazards, Geophysics Monograph 79*, American Geophysics Union, 573-582.

Dixon, M. & Wiener, G. (1993). TITAN: Thunderstorm Identification, Tracking, Analysis, and Nowcasting – A radar-based methodology. *Journal of Atmospheric and Oceanic Technology 10*(6), 785-797.

Done, J., Davis, C., & Weisman, M. (2004). The next generation of NWP: explicit forecasts of convection using the Weather Research and Forecasting (WRF) model. *Atmospheric Science Letters 5*, 110-117.

Dupilka, M. & Reuter, G. (2006). Forecasting tornadic thunderstorm potential in Alberta using environmental sounding data. Part I: Wind shear and buoyancy. *Weather and Forecasting 21*, 325-335.

Einfalt, T., Denoeux, T., & Jacquet, G. (1990). A radar rainfall forecasting method designed for hydrological purposes. *Journal of Hydrology 114*, 229-244.

Elmore, K., Stensrud, D., & Crawford, K. (2002). Explicit cloud-scale models for operational forecasts: A note of caution. *Weather and Forecasting 17*, 873-884.

Environment Canada (EC). (2013). What is a PRECIP product? *Government of Canada* (Last updated 27 November, 2013). Retrieved 31 January, 2015, from http://www.ec.gc.ca/meteo-weather/default.asp?lang=En&n=722A1CDB-1.

Environment Canada (EC). (2014). 25km resolution numerical data of the Global Deterministic Prediction System (GDPS) model – GRIB2 format. *Government of Canada* (Last updated 12 December, 2014). Retrieved 15 January, 2015, from https://weather.gc.ca/grib/grib2_glb_25km_e.html.

Erfani, A., Méthot, A., Goodson, R., Bélair, S., Yeh, K.-S., Côté, J., & Moffet, R. (2003). Synoptic and mesoscale study of a severe convective outbreak with the nonhydrostatic Global Environmental Multiscale (GEM) model. *Meteorology and Atmospheric Physics 82*, 31-53.

Fabry, F., Austin, G., & Tees, D. (1992). The accuracy of rainfall estimates by radar as a function of range. *Quarterly Journal of the Royal Meteorological Society 118*, 435-453.

Flesch, T. & Reuter, G. (2012). WRF model simulation of two Alberta flooding events and the impact of topography. *Journal of Hydrometeorology 13*, 695-708.

Fowle, M. & Roebber, P. (2003). Short-range (0-48 h) numerical prediction of convective occurrence, mode, and location. *Weather and Forecasting 18*, 782-794.

Gill, D. & Pyle, M. (2012). WRF Nesting. *January 2012 Basic WRF Tutorial*, NCAR Foothills Laboratory, Boulder, Colorado, 23-27 January, 2012. Retrieved 17 August, 2012, from http://www.mmm.ucar.edu/wrf/users/tutorial/201201/WRFNesting.ppt.pdf.

Han, L., Fu, S., Zhao, L., Zheng, Y., Wang, H., & Lin, Y. (2009). 3D convective storm identification, tracking, and forecasting – An enhanced TITAN algorithm. *Journal of Atmospheric and Oceanic Technology 26*, 719-732.

Hong, S., Noh, Y., & Dudhia, J. (2006). A new vertical diffusion package with an explicit treatment of entrainment processes. *Monthly Weather Review 134*, 2318-2341.

Joe, P. & Lapczak, S. (2002). Evolution of the Canadian operational radar network. *Proceedings of the European Conference on Radar in Meteorology and Hydrology*, 370-382.

Johnson, J., MacKeen, P., Witt, A., Mitchell, E., Stumpf, G., Eilts, M., & Thomas, K. (1998). The Storm Cell Identification and Tracking Algorithm: An enhanced WSR-88D algorithm. *Weather and Forecasting 13*, 263-276.

Jong-Chul, H., Yong-Hee, L., Dong-Eon, C., Hee-Choon, L., & Hee-Sang, L. (2007). Comparison of precipitation forecasts from MM5, WRF-ARW and WRF-NMM over the Korean Peninsula during summer season. *8th WRF Users' Workshop*, National Center for Atmospheric Research, Boulder, Colorado, 11-15 June, 2007.

Kain, J. & Fritsch, J. (1990). A one-dimensional entraining/detraining plume model and its application in convective parameterization. *Journal of the Atmospheric Sciences 47*(23), 2784-2802.

Kain, J. & Fritsch, J. (1993). Convective parameterization for mesoscale models: The Kain-Fritsch scheme. *Meteorological Monographs 24*(46), 165-170.

Kain, J. (2004). The Kain-Fritsch convective parametrization: An update. *Journal of Applied Meteorology 43*, 170-181.

Kain, J., Weiss, S., Levit, J., Baldwin, M., & Bright, D. (2006). Examination of convection-allowing configurations of the WRF model for the prediction of severe convective weather: The SPC/NSSL Spring Program 2004. *Weather and Forecasting 21*(2), 167-181.

Kain, J., Weiss, S., Bright, D., Baldwin, M., Levit, J., Carbin, G., Schwartz, C., Weisman, M., Droegemeier, K., Weber, D., & Thomas, K. (2008). Some practical considerations regarding horizontal resolution in the first generation of operational convection-allowing NWP. *Weather and Forecasting 23*, 931-952.

Keighton, S., Lee, L., Holloway, B., Hotz, D., Zubrick, S., Hovis, J., Votaw, G., Perry, L., Lackmann, G., Yuter, S., Konrad, C., Miller, D., & Etherton, B. (2009). A collaborative approach to study northwest flow snow in the southern Appalachians. *Bulletin of the American Meteorological Society 90*(7), 979-991.

Koch, S., Ferrier, B., Stoelinga, M., Szoke, E., Weiss, S., & Kain, J. (2005). The use of simulated radar reflectivity fields in the diagnosis of mesoscale phenomena from high-resolution WRF model forecasts. *Preprints, 11th Conference on Mesoscale Processes, Albuquerque, New Mexico, American Meteorological Society, J4J.7*.

Krauss, T. & Sinkevich, A. (2007A). Investigation of Cb motion in the province of Alberta (Canada). *Russian Meteorology and Hydrology 32*(2), 93-101.

Krauss, T. & Sinkevich, A. (2007B). Investigation of severe storm motion. *9th WMO Scientific Conference on Weather Modification*, Antalya, Turkey, 22-25 November, 2007. World Meteorological Organization.

Kuster, C., Burke, P, & Taylor, A. (2012). An 11-year radar-based study of tornadic thunderstorms over central Oklahoma. *Electronic Journal of Severe Storms Meteorology 7*(8), 1-18.

Lin, Y., Farley, R., & Orville, H. (1983). Bulk parameterization of the snow field in a cloud model. *Journal of Climate and Applied Meteorology 22*, 1065-1092.

Maddox, R. (1976). An evaluation of tornado proximity wind and stability data. *Monthly Weather Review 104*, 133-142.

Marshall, J., Langille, R., & Palmer, W. (1947). Measurement of rainfall by radar. *Journal of Meteorology 4*, 186-192.

McMurray, J. (2010). Hailstorm costliest in Canadian history. *Calgary Sun*, [online] (Last updated 11:13 PM MDT 11 August 2010). Retrieved 17 August, 2012, from http://www.calgarysun.com/news/alberta/2010/08/11/14990491.html.

Michalakes, J., Dudhia, J., Gill, D., Klemp, J., & Skamarock, W. (1999). Design of a next-generation regional weather research and forecast model. *Towards Teracomputing*, World Scientific, River Edge, New Jersey, 117-124.

Milbrandt, J. & Yau, M. (2006). A multimoment bulk microphysics parameterization. Part III: Control simulation of a hailstorm. *Journal of the Atmospheric Sciences 63*, 3114-3136.

Mohee, F. & Miller, C. (2010). Climatology of thunderstorms for North Dakota, 2002-06. *Journal of Applied Meteorology and Climatology 49*, 1881-1890.

National Severe Storms Laboratory (NSSL). (2006). A severe weather primer: Questions and answers about thunderstorms – Forecasting thunderstorms. *National Oceanic and Atmospheric Administration* (Last updated 16 November, 2006). Retrieved 20 August, 2012, from http://www.nssl.noaa.gov/primer/tstorm/tst_predicting.html.

Ogrodnik, I. (2013). By the numbers: 2013 Alberta floods. *Shaw Media*, [online] (Last updated 5:21 AM MDT 27 June, 2013). Retrieved 27 May, 2015, from http://globalnews.ca/news/673236/by-the-numbers-2013-alberta-floods/.

Paruk, B.J. & Blackwell, S.R. (1994). A severe thunderstorm climatology for Alberta. *National Weather Digest 19*(1), 27-33.

Patrick, D. & McCarthy, P. (2008). Improved thunderstorm detection, tracking and assessment products for Environment Canada radars. *24th Conference on Severe Local Storms*, Savannah, Georgia, 27-31 October, 2008.

Pennelly, C. (2013). Verification of the Weather Research and Forecasting model for Alberta. M.Sc. Thesis, University of Alberta, Edmonton, Canada, 89 pp.

Public Weather Services (PWS). (2012). Nowcasting. *World Meteorological Organization*. Retrieved 15 August, 2012, from http://www.wmo.int/pages/prog/amp/pwsp/Nowcasting.htm.

Rasmussen, E. & Blanchard, D. (1998). A baseline climatology of sounding-derived supercell and tornado forecast parameters. *Weather and Forecasting 13*, 1148-1164.

Research Applications Laboratory (RAL). (2012). TITAN – Thunderstorm Identification, Tracking, Analysis, and Nowcasting. *National Center for Atmospheric Research* (Last updated 9:50:44 MST 16 February, 2012). Retrieved 20 August, 2012, from http://www.ral.ucar.edu/projects/titan/home/.

Rozumalski, R. (2006). NWS SOO STRC EMS User's Guide. Available online at http://strc.comet.ucar.edu/software/newrems/.

Schwartz, C., Kain, J., Weiss, S., Xue, M., Bright, D., Kong, F., Thomas, K., Levit, J., & Coniglio, M. (2009). Next-day convection-allowing WRF model guidance: A second look at 2-km versus 4-km grid spacing. *Monthly Weather Review 137*, 3351-3372.

Shuman, F. (1989). History of numerical weather prediction at the National Meteorological Center. *Weather and Forecasting 4*, 286-296.

Sioutas, M. & Flocas, H. (1996). Influence of environmental winds on propagation and motion of thunderstorms in northern Greece. *Journal of Geophysical Research 101*(D21), 26255- 26265.

Skamarock, W., Klemp, J., Dudhia, J., Gill, D., Barker, D., Duda, M., Huang, X., Wang, W., & Powers, J. (2008). A description of the Advanced Research WRF version 3. *NCAR Technical Note* NCAR/TN-475+STR, 113 pp.

Smith, S. & Yau, M. (1993). The causes of severe convective outbreaks in Alberta. Part II: Conceptual model and statistical analysis. *Monthly Weather Review 121*, 1126-1133.

Smith, S., Reuter, G., & Yau, M. (1998). The episodic occurrence of hail in central Alberta and the Highveld of South Africa: Research note. *Atmosphere-Ocean 36*(2), 169-178.

Stensrud, D., Xue, M., Wicker, L., Kelleher, K., Foster, M., Schaeffer, J., Schneider, R., Benjamin, S., Weygandt, S., Ferree, J., & Tuell, J. (2009). Convective-scale warn-on-forecast system: A vision for 2020. *Bulletin of the American Meteorological Society 90*(10), 1487-1499.

The Canadian Press. (2013). Alberta floods costliest natural disaster in Canadian history. *The Canadian Press* (Last updated 7:02 PM MT 23 September, 2013). Retrieved 27 May, 2015, from http://www.cbc.ca/news/canada/calgary/alberta-floods-costliest-natural-disaster-in-canadian-history-1.1864599.

The COMET Program (COMET). (2003). Principles of convection II: Using hodographs. *The COMET© Program* (Last updated 2 December, 2013). Retrieved 12 August, 2015, from http://www.meted.ucar.edu/mesoprim/hodograf/print.php.

Tota, J., Lima, K., Silva, R., & Kuhn, P. (2014). WRF EMS model high resolution simulations over river-urban area in Amazonia. *American Geophysical Union Fall Meeting*, San Francisco, California, 15-19 December, 2014.

Wang, W. & Seaman, N. (1997). A comparison study of convective parameterization schemes in a mesoscale model. *Monthly Weather Review 125*, 252-278.

Watson, L., Hoeth, B., & Blottman, P. (2008). Weather Research and Forecasting model sensitivity comparisons for warm season convective initiation. *Preprints, 22nd Conference on Weather Analysis and Forecasting & 18th Conference on Numerical Weather Prediction, Park City, Utah, American Meteorological Society, J11A.1*.

Weisman, M. & Klemp, J. (1986). Characteristics of isolated convective storms. *Mesoscale Meteorology and Forecasting*, P.S. Ray, Ed., American Meteorological Society, 331-358.

Weisman, M., Skamarock, W., & Klemp, J. (1997). The resolution dependence of explicitly modeled convective systems. *Monthly Weather Review 125*, 527-548.

Western Direct Insurance. (2014). The most expensive and deadly hailstorms in Alberta's history. *Western Direct Insurance News and Advice* (Last updated 18 June, 2012). Retrieved 31 January, 2015, from https://www.westerndirect.ca/learning-centre/insurance-news-and-advice/view/788-the-most-expensive-and-deadly-hailstorms-in-alberta-s-history.

Wilhelmson, R. & Klemp, J. (1978). A numerical study of storm splitting that leads to long-lived storms. *Journal of the Atmospheric Sciences 35*, 1974-1986.

Wilson, J. & Kessler III, E. (1963). Use of radar summary maps for weather analysis and forecasting. *Journal of Applied Meteorology 2*(1), 1-11.

Xin, L., Reuter, G., & Larochelle, B. (1997). Reflectivity –rain rate relationships for convective rainshowers in Edmonton: Research note. *Atmosphere-Ocean 35*(4), 513-521.

Yang, Y. & King, P. (2010). Investigating the potential of using radar echo reflectivity to nowcast cloud-to-ground lightning initiation over southern Ontario. *Weather and Forecasting 25*, 1235-1248.

Zavodsky, B., Case, J., Gotway, J., White, K., Medlin, J., Wood, L., & Radell, D. (2014). Development and implementation of dynamic scripts to support local model verification at National Weather Service Weather Forecast Offices. *94th American Meteorological Society Annual Meeting*, Atlanta, Georgia, 2-6 February, 2014.

Zeitler, J. & Bunkers, M. (2005). Operational forecasting of supercell motion: Review and case studies using multiple datasets. *National Weather Digest 29*(1), 81-97.

Appendices

Appendix A: Hail size conversion table

Table A-1. Environment Canada's Severe Weather Event Database (SWED) hail size conversion table.

Hail Size as referenced to an Object	Hail Diameter (mm)
Shot	1-3
Pea	4-7
Marble	7-15
Grape	15-20
Dime	18
Penny	19
Nickel	21
Quarter	24
Loonie	27
Toonie	29
Walnut	35
Golf ball	45
Hen egg	50
Tennis ball	64
Baseball	70
Tea cup	75
Grapefruit	102
Softball	115

Appendix B: Calculating mean wind

The following steps are used to calculate the 0-6 km mean wind and plot it on a hodograph (COMET 2003).

1) Move the origin of the hodograph to the point representing the surface wind if it is not already at the origin.
2) Rotate the x and y axes so that the x axis passes through the point representing the 6 km wind.
3) Separately average the u and v components of the wind from the surface to 6 km, referring to the new reference frame.
4) Add the u and v vectors and plot a point at this location on the hodograph within the new reference frame.
5) Draw a line from the origin of the original reference frame to this point. This is the 0-6 km mean wind vector.

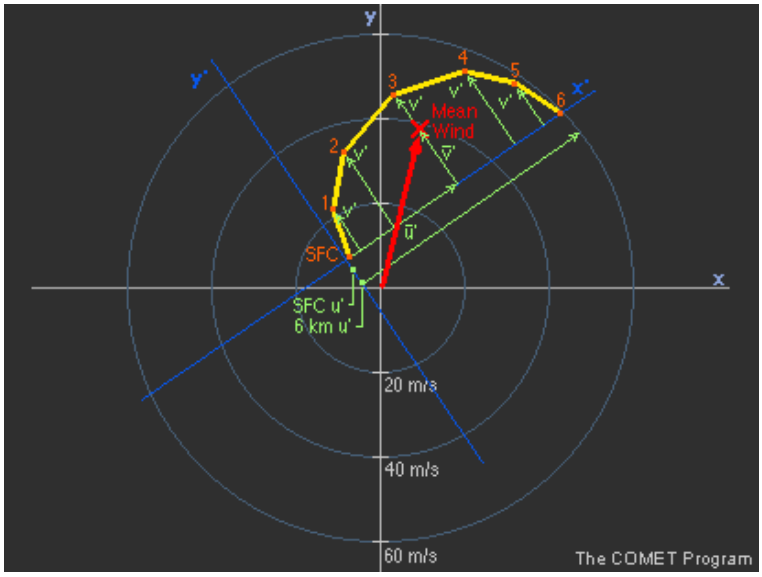

Figure B-1. An example of a curved hodograph with wind velocity from the surface to 6 km. The calculated 0-6 km mean wind vector is in red. In this case the x and y axes needed to be moved and rotated to find the mean wind. The original reference frame is in light blue and the rotated reference frame is in dark blue. The $\overline{u}'$ and $\overline{v}'$ vectors in green represent the components of the mean wind within the rotated reference frame (COMET 2003).

Appendix C: Bunkers Method

The following steps are used to find the forecast storm motion for left- and right-moving supercells using Bunkers Method on a hodograph (Bunkers et al. 2000, Bunkers 2002).

1) Plot the 0-6 km mean wind on the hodograph (Appendix B).
2) Draw the 0-0.5 km to 5.5-6 km vertical wind shear vector on the hodograph.
3) Draw a line perpendicular to the vertical wind shear vector that passes through the mean wind.
4) Plot a point on the line that has a 7.5 m/s (15 kt) deviation to the right of the mean wind. This is the forecast storm motion for a right-moving supercell.
5) Plot a point on the line that has a 7.5 m/s (15 kt) deviation to the left of the mean wind. This is the forecast storm motion for a left-moving supercell.

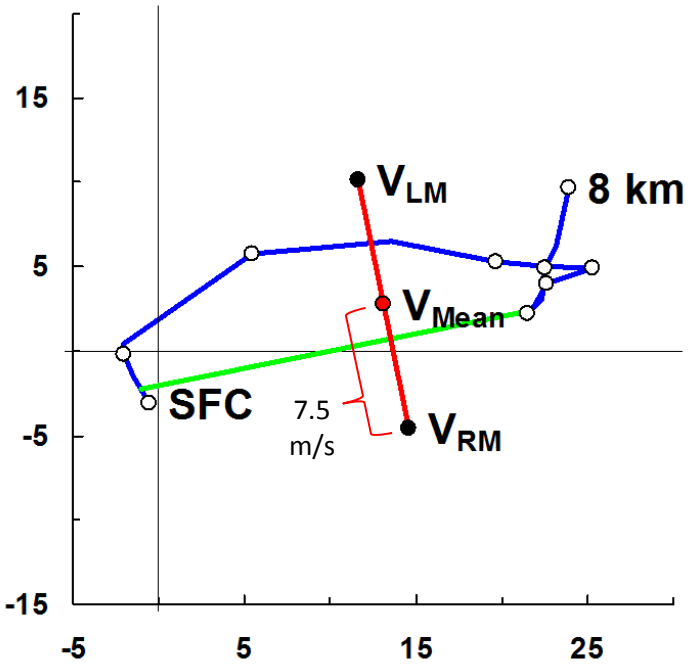

Figure C-1. An example of a hodograph with wind velocity (m/s) from the surface to 8 km. The 0-6 km mean wind (V_{Mean}), Bunkers left-moving supercell velocity (V_{LM}), and Bunkers right-moving supercell velocity (V_{RM}) are plotted on the hodograph. The green line is the 0-0.5 km to 5.5-6 km vertical wind shear vector and the red line is perpendicular to the wind shear vector. The x and y axes of the hodograph are in m/s (Bunkers 2002).